Nanoarchitectonics of a microsphere-based scaffold for modeling neurodevelopment and neurological disease

Eric S. Sandhurst[a,b], Sharad V. Jaswandkar[c], Krishna Kundu[c], Dinesh R. Katti[c], Kalpana S. Katti[c], Hongli Sun[a,b#], Daniel Engebretson[a], Kevin R. Francis[a,b,d,e*#]

[a] Department of Biomedical Engineering, University of South Dakota, Sioux Falls, SD, USA.

[b] BioSystems Networks and Translational Research Center, Brookings, SD, USA.

[c] Civil, Construction and Environmental Engineering Department, North Dakota State University, Fargo, ND, USA.

[d] Cellular Therapies and Stem Cell Biology Group, Sanford Research, Sioux Falls, SD, USA.

[e] Department of Pediatrics, University of South Dakota Sanford School of Medicine, Sioux Falls, SD, USA.

[*] Corresponding author: K. R. F. (kevin.francis@sanfordhealth.org).

[#] Lead Contact: K.R.F. (kevin.francis@sanfordhealth.org)

Keywords: three-dimensional, scaffold, differentiation, neurodevelopment, induced pluripotent stem cell

Abstract

Three-dimensional (3D) cellular constructs derived from pluripotent stem cells allow the *ex vivo* study of neurodevelopment and neurological disease within a spatially organized model. However, the robustness and utility of 3D models is impacted by tissue self-organization, size limitations, nutrient supply, and heterogeneity. Herein, we have utilized the principles of nanoarchitectonics to create a multifunctional, polymer/bioceramic composite microsphere system for stem cell culture and differentiation in a chemically defined microenvironment. Microspheres could be customized to produce three-dimensional structures of defined size (ranging from <100 to >350 μm) with lower mechanical properties compared to thin-film. Further, microspheres softened in solution, approaching more tissue-like mechanical properties with time. Using neural stem cells (NSCs) derived from human induced pluripotent stem cells, microsphere-cultured NSCs were able to utilize multiple substrates to promote cell adhesion and proliferation. Prolonged culture of NSC-bound microspheres in differentiating conditions promoted the formation of both neural and glial cell types from control and patient-derived stem cell models. Human NSCs and differentiated neurons could also be co-cultured with astrocytes and human umbilical vein endothelial cells (HUVECs), demonstrating possible application for tissue-engineered modeling of development and human disease. We further demonstrate microspheres allow the loading and sustained release of multiple recombinant proteins to support cellular maintenance and differentiation. While previous work has principally utilized self-organizing models or protein-rich hydrogels for 3D neural culture, the three-dimensional matrix presented here represents a chemically defined and robust alternative for the *in vitro* study of neurodevelopment and nervous system disorders.

Keywords: microsphere, scaffold, three-dimensional, induced pluripotent, iPSC, NSC

Graphical Abstract

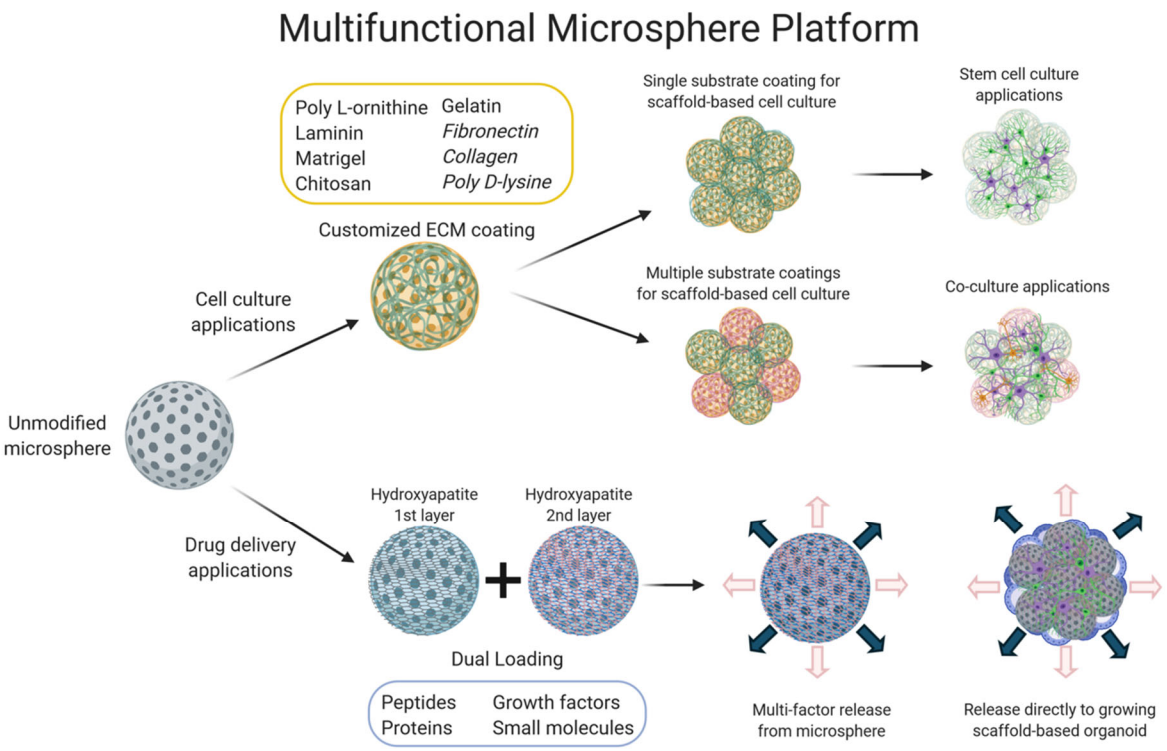

Introduction

Disorders affecting the nervous system are one of the leading causes of co-morbidity and death worldwide.[1, 2] Observing and analyzing disease impacts on the nervous system is inherently challenging within affected individuals. The use of model systems to recapitulate different structures and functions of the nervous tissue under study provides a mechanism to study neurological disease. Many of the insights into neuropathological disease have come from research on post-mortem tissue, traditional two-dimensional (2D) cell culture experiments, and within animal models such as transgenic mice and rats. Despite the availability of genetic and technological tools and a robust foundation of neuroscience research, these model systems each have limitations.[3] Studying the pathogenesis of complex diseases has proven to be particularly difficult due to a lack of access to healthy and diseased brain tissue, immature and spatially limited *in vitro* cell culture systems, and animal models that fail to capture the developmental, architectural, and species-specific aspects of the human brain.[2, 4] Therefore, additional models of the human nervous system are needed to help overcome some of these limitations.

Human induced pluripotent stem cells (iPSCs) have created a fundamental shift in how scientists study human disease. By establishing a reliable method for generating individual-specific pluripotent cells, iPSCs represent a robust model system for the study of human disease and may accelerate progress towards revolutionary treatments.[5] iPSC-derived neural stem cells (NSCs), therefore, are a useful tool to provide insights into the underlying mechanisms of neurodevelopment and neurodegenerative diseases. The use of iPSCs has led to new strategies for therapeutic intervention and increased accuracy for drug discovery.[6-9] Although iPSCs represent a revolution in studying development and human disease *in vitro*, researchers have predominantly relied on 2D culture platforms.[10] Since traditional monolayer cultures support only planar cell-cell interaction, this system poorly simulates the natural three-dimensional (3D) microenvironment of the body. The natural interaction and communication between the heterogeneous milieu of cells and the extracellular matrix found within the body is difficult to replicate in 2D culture.[11] Certain cellular characteristics, including apicobasal polarity and guided cell migration, cannot be recapitulated in planar culture systems.[12] Spatially complex iPSC models of neurological disease are thus needed.[13]

As recent groundbreaking studies have shown, 3D culture of iPSCs more accurately represents the spatial arrangement and temporal development of nervous tissue when compared to 2D models.[3, 14-16] Research conducted with 3D culture models provides new knowledge of areas that were previously only poorly modeled or inaccessible altogether, such as the cerebral cortex,

neocortex, ventral forebrain, ventral telencephalon, cerebellum, midbrain, choroid plexus, and optic cup.[14-19] Although each 3D protocol has advantages and disadvantages, they all utilize the capacity of embryonic stem cells or iPSCs to self-organize, self-assemble, and differentiate within a 3D environment.[2] Known as spheroids, neurospheres, cellular scaffolds or organoids depending on their complexity and the methods used, these 3D platforms can produce functional, highly-organized populations of cells.[1, 20, 21] However, 3D models are still limited by experimental heterogeneity, limited control over tissue organization, inadequate diffusion and heterogeneous distribution of macromolecules, and endpoint analyses.[17, 22-29]

To help overcome the limitations of current 3D models, we have developed a microsphere-based scaffold with nanoarchitectural features for iPSC-based neural differentiation[30, 31]. Using a biomaterial-based microenvironment, we have created an alternative to the undefined components present within other materials-based 3D culture systems. We have defined the mechanical properties of this scaffold, demonstrated the maintenance and lineage differentiation of iPSC-derived NSCs cultured on the scaffold, established a protocol for co-culture of multiple neural and endothelial cell types, and utilized this scaffold for localized cellular delivery of small molecules. This system represents a novel advancement in 3D culture and provides a multifunctional platform for disease modeling, drug screening applications, and developmental studies.

Materials and methods

Chemicals and reagents

Poly lactic-co-glycolic acid (PLGA; 50:50, 1.15 dL/g) was purchased from Lactel (Birmingham, AL). Gelatin Type A, dichloromethane, poly L-ornithine, molecular grade water, bovine serum albumin (BSA), disodium ethylenediaminetetraacetate (EDTA), and magnesium chloride were purchased from Sigma Aldrich (St. Louis, MO). Low-attachment 24-well plates, sodium chloride, sodium bicarbonate, Tris base, Neurobasal media, and epidermal growth factor were purchased from ThermoFisher Scientific (Carlsbad, CA). B27 supplement with vitamin A, B27 without vitamin A, Accutase and Glutamax were all purchased from Life Technologies (Carlsbad, CA). Basic fibroblast growth factor (bFGF) was purchased from Reprocell (Beltsville, MD). Y27632 ROCK inhibitor was purchased from Reagents Direct (Encinitas, CA). mTeSR1 was purchased from Stem Cell Technologies (Vancouver, BC). DMEM, DMEM-F12, Penicillin/streptomycin, One Shot fetal bovine serum, Trypsin-EDTA, and phosphate buffered saline were purchased from Gibco (Carlsbad, CA). BDNF and GDNF were purchased from Peprotech (Rocky Hill, NJ). Matrigel

hESC-Qualified Matrix was purchased from Corning (Glendale, AZ). Laminin was purchased from Invitrogen (Carlsbad, CA). Hydrochloric acid was purchased from Avantor Performance Materials (Center Valley, PA). Polyvinyl alcohol was purchased from PolySciences, Inc. (Warrington, PA). Ethanol, calcium chloride, and sodium phosphate were purchased from Acros Organics (Fair Lawn, NJ). 96-well ultra-low attachment plates were purchased from Nexcelom Bioscience (Lawrence, MA).

Preparation of microspheres

A double emulsion procedure was used to prepare porous microspheres. First, 0.5 g of 50:50, 1.15 viscosity PLGA was placed into a glass vial with 15 mL of dichloromethane (DCM). PLGA was dissolved under constant stirring at 700 rpm at 50 °C. Simultaneously, the primary aqueous phase was prepared by dissolving 0.4 g of type A porcine gelatin and 5 mg of polyvinyl alcohol (PVA) in 5 mL of deionized (DI) water in a separate glass vial. A third solution, the secondary aqueous phase, was prepared by dissolving 200 mg of PVA in 200 mL of DI water and cooled to 4 °C. The dissolved polymer solution was poured into a 25 mL beaker and placed on a hotplate at 50 °C under the IKA homogenizer (IKA Works, Inc., Wilmington, NC). The aqueous solution was added manually using a 1000 µL pipette and the two solutions were emulsified for 5 min at 4000 rpm. The primary emulsion was immediately poured into the secondary aqueous phase and rotated using a magnetic stir plate at 400 rpm for 60 min. After stirring at 400 rpm for 60 min, the contents of the beaker were poured into 1200 mL of fresh DI water and stirred overnight at 300 rpm to facilitate DCM evaporation. The supernatant was discarded, the microspheres were rinsed and collected in a 50 mL conical tube, kept at -80 °C for 60 min, and lyophilized for 36 - 48 h. Following lyophilization, microspheres were treated with an ethanolic sodium hydroxide solution at a ratio of 20% 1M NaOH and 80% pure ethanol.[32] Microspheres were placed into a 50 mL conical tube and vortexed for 20 - 30 s. Microspheres were rinsed with DI water, collected in a nylon cell strainer, kept at -80 °C freezer for 60 min, and lyophilized for 36 - 48 h.

Hydroxyapatite deposition on microspheres

The mineralization process of PLGA microsphere scaffolds was performed as previously published.[33] Briefly, microspheres were divided into fractions based on diameter (ex: 150 - 300 µm) by filtering them through ATSE metal sieves of decreasing size. Hydroxyapatite (HA) was formed on the entire exposed surface of the microsphere structure during two phases of immersion into two solutions known as simulated body fluid (SBF). First, microspheres were immersed into a phase I nucleation solution (P1). For P1, 19.95 g of NaCl, followed by 0.69 g of

$CaCl_2$, 0.45 g of $NaHPO_4$, 0.88 g of $NaHCO_3$, and 0.76 g of $MgCl_2$ were dissolved in 500 mL DI water under stirring conditions. 25 mg of microspheres, with a diameter of 150 - 300 µm, were placed into a glass vial and 25 mL of P1 nucleation solution was added to the vial. Each vial was placed into an orbital shaker, heated to 37 °C, and set for 100 rpm for 12 h. To verify P1 deposition, a FITC-labeled scrambled peptide (FITC-QEQLERALNSS, Biomatik) was added to the P1 SBF and imaged by confocal microscopy.[34]

After 12 h, microspheres were collected in a nylon cell strainer, kept at -80 °C for 60 min, and lyophilized for 18 - 24 h. Next, a phase II propagation solution (P2) was created by dissolving various salts. First, 0.27 g of $CaCl_2$, followed by 3.98 g of NaCl, and 0.175 g of $HaHPO_4$ were dissolved in 497.5 mL of DI water and 2.5 mL of 10M HCl under stirring conditions. Tris buffer was added to achieve a pH of 7.4. P1 microspheres were placed in a new glass vial and 25 mL of P2 propagation solution was added to the vial. Each vial was placed into an orbital shaker, heated to 35° C, and set for 100 rpm for 12 h. The microspheres were then collected in a nylon cell strainer, kept at -80 °C for 20 min, and lyophilized for 18 - 24 h. To verify P2 deposition, BSA conjugated to AlexaFluor647 (Invitrogen, Carlsbad, CA) was added to P2 SBF and imaged by confocal microscopy.

Poly-L-ornithine (PLO) and laminin coating of 2D and 3D surfaces

0.2% (v/v) PLO diluted in molecular grade water was added to culture surfaces and allowed to conjugate for 12 h in a 37 °C incubator. Dishes were rinsed twice with molecular grade water before a 1% solution (v/v) of natural mouse laminin diluted in PBS was added to each well. Culture dishes were incubated at 37 °C for 12 h and either used immediately or stored at -20 °C. Microspheres were immersed in 0.2% (v/v) PLO and placed in an enclosed orbital shaker maintained at 37 °C and 100 rpm for 12 h. Microspheres were rinsed twice with molecular grade water and placed into a new glass vial, immersed in a 1% solution of natural mouse laminin and placed in an enclosed orbital shaker set for 37 °C and 100 rpm for 12 h. PLO+laminin coated microspheres were kept at 4 °C and used within 12 h.

Ultra-structural characterization of microspheres

A FEI Quanta 450 field-emission scanning electron microscope (SEM) was used to characterize the morphological structures of microsphere samples. Overall microsphere diameter was analyzed using SEM images. Micro CT was performed by ScanCo Associates, (ScanCo µCT 50, Brüttisellen, Switzerland) to measure local pore diameter. Microsphere porosity was calculated

using micro CT imaging, performed by ScanCo Associates. Microsphere porosity was determined using the following equation:

$$P_{scaffold} = \frac{V - V_P}{V} \times 100\%$$

where $P_{scaffold}$ is the porosity of the microsphere batch, V is the total volume of the microsphere batch, and V_p is the volume of PLGA is equal to the mass divided by the density of PLGA (ρ = 1.3 g/cm^3).

Nanomechanical evaluation of microspheres

To prepare a PLGA film for mechanical testing, 0.5 g of 50:50 PLGA (3.3% (w/v)), 0.75 g of 50:50 PLGA (5% (w/v)) and 1 g of 50:50 PLGA (6.6% (w/v)) were each dissolved in 15 mL DCM and poured into a 25 mL glass beaker. Once the solvent evaporated, testing coupons were cut from each film and attached to titanium metal sections (10 mm x 10 mm x 0.25 mm) (Sigma, St. Louis, MO) with 100 µl Elmer's glue (Westerville, OH). To prepare PLGA microspheres samples for nanomechanical testing, 100 µl of Minwax polyacrylic (Upper Saddle River, NJ) was first applied to titanium sections using a spin coating system. A Dremel rotary tool (Dremel, Racine, WI) was used at 10,000 rpm for 5s to obtain a uniform polyacrylic layer before adherence of microspheres or films to the substrates is achieved. Samples were allowed to dry completely. Prior to nanoindentation experiments, some samples were rehydrated in neurobasal media for 1d, 2d, or 7d. Samples were removed from the aqueous phase and carefully blotted before nanoindentation.

A Hysitron Triboindenter (Hysitron Inc., Minneapolis, MN, USA) nanoindenter with a pyramidal Berkovich diamond indenter tip (tip radius of 200 nm) was used to calculate the mechanical properties of three PLGA films (3.3% (w/v), 5% (w/v), 6% (w/v)) and PLGA microspheres (3.3% (w/v) in dry and hydrated states. After calibration with a standard fused quartz reference sample, an indentation depth was set at 1000 nm with a 20 nm/s displacement rate. The elastic modulus and hardness of each sample were measured at room temperature. A displacement depth of 1000 nm was selected for all quasistatic nanoindentation experiments, resulting in reliable elastic property measurements free of substrate effects. Average values of elastic modulus and indentation hardness were calculated from the analysis of 30 unique microspheres. The estimation methods for determining elastic modulus (E) and indentation hardness (H_{IT}) were based on Oliver and Pharr's methods.[35-38] These methods have been applied to make direct nanoindenter-based measurements of elastic and inelastic properties of soft materials such as human cells.[39, 40]

Fourier Transform Infrared Spectroscopy (FTIR) analysis

Transmission FTIR spectroscopy studies were performed using samples of polyvinyl alcohol (PVA), gelatin, PLGA, microspheres, microspheres coated with HAP for 12 h, and microspheres coated with HAP for 24 h. Samples were sandwiched between two KBr windows and placed in a universal sample holder. A Thermo Nicolet, Nexus, 870 spectrometer equipped with a KBr beam splitter was used for performing these experiments in the range of 4000 – 960 cm^{-1}. A spectral resolution of 4 cm^{-1} and 32 scans were used for each sample.

Culture of human iPSCs, NSCs, and neural differentiation

Two control human iPSC lines, NL5 (NCRM-5; kind gift from the iPSC Core Facility, NHLBI, Bethesda, MD) and Scui21 (Scui; kind gift from the NIH Stem Cell Unit, NINDS, Bethesda, MD), and one Smith-Lemli-Opitz syndrome (SLOS) patient-derived iPSC line (CWI 4F2; kind gift from Dr. Forbes Porter, NICHD, Bethesda, MD) were cultured and directed towards NSCs using a rosette-based assay as previously published.[41, 42] Following their derivation and expansion, NSCs were cultured on PLO+laminin coated 35 mm tissue culture dishes in NSC media (DMEM, 2 mM glutamine, B27 minus vitamin A, 20 ng/mL EGF, 20 ng/mL bFGF, 50 µg/mL Penicillin-streptomycin) supplemented with ROCK inhibitor Y27632 (10 µM). Media was changed every other day. Cells were passaged via incubation with Accutase (Life Technologies, Carlsbad, CA) at 37 °C for 3 - 5 min. Enzymatic reaction was stopped by adding NSC culture media with Y27632, followed by centrifugation at 1,500 rpm. Cells were divided evenly between two new PLO+laminin coated culture dishes (approximately 2.5 – 3 x 10^6 cells per dish).

To induce neural differentiation, NSCs were collected from 35 mm cell expansion dishes as described above. Upon resuspension in NSC media, cells were plated in 24- or 96-well plates coated with PLO+laminin (ThermoFisher Scientific, Waltham, MA) or Lab-Tek Nunc 4-well chamber glass slides coated with PLO + laminin. Cells were maintained in NSC media supplemented with 10% fetal bovine serum (FBS) for 4 days and then changed to neural differentiation media (Neurobasal media, B27 with vitamin A, 10 ng/mL GDNF, 10 ng/mL BDNF, 2 mM glutamine, 50 µg/mL penicillin-streptomycin) for the duration of differentiation. For neurosphere culture, NSCs were collected via Accutase and plated at 150,000 cells per well in a 96-well, round-bottom ultra-low attachment plate. Neurospheres were maintained in suspension in NSC media supplemented with FBS for 4 days and then changed to NSC differentiation media for the duration of each experiment. For microsphere culture of NSCs, 100 µg of microspheres were added to each round-bottom well of an ultra-low attachment 96-well plate. Upon

resuspension in NSC media, 150,000 cells were passively seeded onto the microspheres. Microspheres were cultured in NSC media supplemented with FBS for 4 days and then changed to neural differentiation media for the duration of each experiment. All culture plates and dishes were cultured at 37 °C with 5% CO_2.

Serum impact on NSC microsphere attachment

Microspheres were immersed in 70% ethanol for 60 min on an orbital shaker set at 100 rpm. Microspheres (1 mg) were transferred to flat-bottom, low-attachment 24-well plate before NSCs were seeded onto microspheres (150,000 cells per 1 mg of microspheres per well) in NSC media. Serum supplemented groups received 10% FBS. The cells/scaffolds were cultured in a 24-well plate at 37° C with 5% CO_2.

Evaluation of substrates for NSC microsphere attachment

Microspheres were divided into fractions and sterilized as previously mentioned. Microspheres were coated with PLO + laminin as above. Microspheres receiving Matrigel coating were placed into a sterile glass vial and incubated in either Matrigel for 2 h on an orbital shaker set for 50 rpm at room temperature. Uncoated or substrate coated microspheres were transferred to wells of a 24-well plate before NSC control line cells were seeded into the scaffold (150,000 cells per 1 mg of microspheres). Cells/scaffolds were cultured in a 24-well plate at 37 °C with 5% CO_2.

Astrocyte generation from iPSC-derived NSCs

70,000 NSCs were plated onto 35 mm PLO+laminin coated tissue culture dishes and maintained in neural differentiation at 37 °C with 5% CO_2 through d14. On d14, cells were collected via Accutase, transferred to 35 mm tissue culture plates coated with 25 µg/mL poly D-lysine (PDL) (Sigma Aldrich, St. Louis, MO), and media was changed to astrocyte differentiation media (DMEM/F12, 2 mM Glutamine, 10% FBS, and 1% penicillin-streptomycin). Media changes occurred every 48 h through d28. On d28, cells were collected with 0.25% Trypsin-EDTA and transferred to a PDL-coated T25 tissue culture flask for expansion. Astrocytes were expanded and passaged with Trypsin-EDTA for an additional 30 – 45 days as needed prior to use.

Human umbilical vein endothelial cell (HUVEC) microsphere culture

HUVECs obtained from Lonza (Walkersville, MD) were plated on T25 flasks and cultured with Endothelial Basal Medium-2 (cat# 00190860) (Lonza, Walkersville, MD) at 37 °C with 5% CO_2.[34] HUVECs were harvested from the flask by rinsing with PBS, adding 2 mL of 0.05% Trypsin-EDTA to the flask, and incubating at 37° C for 3-5 min. Cells were centrifuged at 1,500 rpm for 5 min,

supernatant was aspirated, and the cell pellet was resuspended in neural differentiation media before adding to microspheres.

Multilineage co-culture using microsphere scaffolds

Microsphere samples were immersed in 70% ethanol for 60 min on an orbital shaker set at 100 rpm. Microspheres (100 µg) were added to each well of an ultra-low attachment 96-well plate. On d0, NSCs were collected from 35 mm cell expansion dishes via Accutase as described above. Upon resuspension, NSCs were passively seeded onto 100 µg of microspheres. On d2, astrocytes were passively seeded onto the NSC-only microspheres. On d5, HUVECs were added to each NSC+astrocyte scaffold. All groups were cultured in NSC differentiation media at 37 °C with 5% CO_2.

Immunofluorescent imaging of scaffold cultured cells

The cell lineage of differentiating NSCs was visualized by immunofluorescence using primary and secondary antibodies. Cell-based spheroids and cell-seeded microspheres were fixed in 4% paraformaldehyde for 20 min, rinsed with 1x PBS, and permeabilized with 0.1% TritonX-100 for 20 min. Samples were subsequently blocked with 5% bovine serum albumin containing 0.1% TritonX-100 in PBS for 60 min before the following primary antibodies were added: chicken anti-GFAP (Novus Biologicals, NBP1-05198, 1:2000), mouse anti-βIII-Tubulin (Millipore, MAB1637, 1:1000), mouse anti-human Nestin (Millipore, MAB5326, 1:2000), mouse anti-MAP2 (Synaptic Systems, 188 011, 1:2000), rabbit anti-Neurofilament, medium chain (Novus Biologicals, NB300-133, 1:2000), rabbit anti-SOX2 (Cell Signaling, 3579S, 1:400), mouse anti-Ki67 (Abcam, ab15580, 1:2000), mouse anti-CD31 (Abcam, ab9498, 1:1000). Samples were incubated with primary antibody at 4 °C overnight. Following overnight incubation, samples were incubated for 60 min with the following secondary antibodies diluted in blocking buffer: AlexaFluor 555 rabbit anti-mouse IgG (Life Technologies, A21427), AlexaFluor 555 donkey anti-rabbit IgG (Life Technologies, A31572), AlexaFluor 488 goat anti-mouse IgG (Life Technologies, A11001), AlexaFluor 488 goat anti-rabbit IgG (Life Technologies, A11008), or AlexaFluor 488 goat anti-chicken IgG (Life Technologies, A11039). All secondaries were diluted 1:500. After rinsing, Fluoromount-G with DAPI was added. Samples were imaged using a confocal laser scanning microscope (Olympus Fluoview FV1200, Olympus, Japan).

Hematoxylin and eosin staining of scaffold cultures

Scaffolds were fixed in 10% neutral buffered formalin and processed on a Leica 300 ASP tissue processor. Tissues were embedded in paraffin and serially sectioned at 5 µm thickness. Slides were stained with hematoxylin and eosin on a Sakura Tissue-Tek automated H&E staining instrument. The program runs as follows: de-paraffinize and rehydrate tissue, stain in Gill's III hematoxylin, differentiate with running tap water, blue in ammonia water, counterstain in eosin, and dehydrate and clear. All images were taken on a Nikon NiE microscope using a Nikon DS-Fi2 camera and 20x/0.75 PlanApo λ objective.

Bovine serum albumin (BSA) loading and release from microspheres

Microspheres were coated with HA as discussed above with minor changes. BSA (2.5 mg) was added to 25 mL of SBF in each combination (+P1-P2; -P1+P2; +P1+P2) and incorporated into the HA. When the microspheres were collected after each HA deposition phase, the supernatant was saved to analyze BSA remaining in the solution. Microspheres were also rinsed with 1 mL of DI water and the rinse solution was saved to calculate incorporation efficiency. To measure the amount of BSA incorporated into the HA microspheres, four groups of BSA-loaded microspheres were immersed in 0.5M EDTA solution and vortexed for 1 min and centrifuged at 2,000x G for 2 min. Incorporation efficiency was determined by calculating the BSA remaining in the SBF supernatant, the BSA in the rinse solution, and the BSA released from microspheres. To model release, 10 mg of BSA-HA microspheres were added to microcentrifuge vials with 1 mL PBS and placed into an incubating shaker set for 100 rpm and 37 °C. At predetermined time points (30 min, 1 h, 2 h, 5 h, 12 h, d1, d2, d3, d7, d10, and d15), 500 µL of PBS eluent was removed and 500 µL fresh PBS was added to the tube. Analysis of BSA release was performed using a Pierce™ bicinchoninic acid (BCA) protein assay kit (Thermo Fisher, Waltham, MA) per manufacturer's instructions.

bFGF loading, release, and impact on cell viability

Microspheres were coated with HA as previously discussed. 20 ng/mL bFGF was added to both SBF phases (+P1+P2) and incorporated into the crystal matrix. NSCs were passively seeded onto 100 µg of microspheres. Microsphere-based scaffolds were cultured in NSC media for 14 days at 37 °C with 5% CO_2. At each time point (d1, d4, d7, and d14), bFGF-HA scaffolds were analyzed by MTS assay to determine the amount of proliferation compared to other 2D and 3D groups. Each group was cultured in triplicate and 50% of the cell culture media was replenished every 48 h. Cell viability was quantitatively analyzed using the CellTiter 96 Aqueous One Solution Cell Proliferation Assay (MTS, Promega, USA) according to the manufacturer's instruction. In brief,

after culturing for 1, 4, 7, or 14 days in round-bottom, ultra-low attachment 96-wells, the culture medium was removed, fresh medium with 10% MTS solution was then added, and incubated at 37 °C with 5% CO_2 in the dark for 1 h. Each biological replicate was analyzed in quadruplicate by removing 100 µL volumes from each well. The absorbance was measured at 490 nm using a microplate reader (Infinite M200, Tecan, USA). Cell viability was expressed as cell number calculated by the slope of a standard curve prepared by culturing NSCs at densities from 50,000 - 500,000 on PLO+laminin coated wells of a 24-well plate (data not shown).

Statistical analyses

To determine the statistical significance of observed differences between the study groups, a two-tailed Student's t-test was applied to the control group and each experimental group. A value of $p<0.05$ was considered to be statistically significant. Values are reported as the mean ± one standard deviation (SD). Microscopic images across treatments were imaged using equivalent laser power and exposure times.

Ethics, human subjects research statement

All research performed using human cell lines was determined to not constitute human subjects research by the institutional review board of Sanford Research.

Results

Preparation of a microsphere scaffold for culture of iPSC derivatives is rapid and tunable

To create a scaffold for culture of iPSC derivatives, we utilized a double emulsion and porogen leaching technique to yield a highly uniform poly(lactic-co-glycolic) (PLGA) microsphere matrix with interconnected pores and >88% overall porosity. Gelatin was utilized as the sacrificial porogen to create spherical pores within the PLGA matrix. Through optimization of each step within the preparation process, we have created a stable, consistent microsphere structure (**Figure 1A**). FTIR analysis of the various materials utilized for microsphere generation and coating was performed to verify production material chemistries in comparison to spectra within the final microsphere product (**Supplemental Figure 1**). Through variations in the speed of mixing the gelatin/PLGA during the emulsion process, we were able to control microsphere diameter (**Figure 1B,C**). Using a 400 rpm mixing step, microsphere diameter exhibited reduced variability and the majority remained within the 100 – 250 µm range (**Figure 1D,E**). Based upon a mean microsphere diameter achieved, we utilized a 400 rpm mixing speed for all subsequent

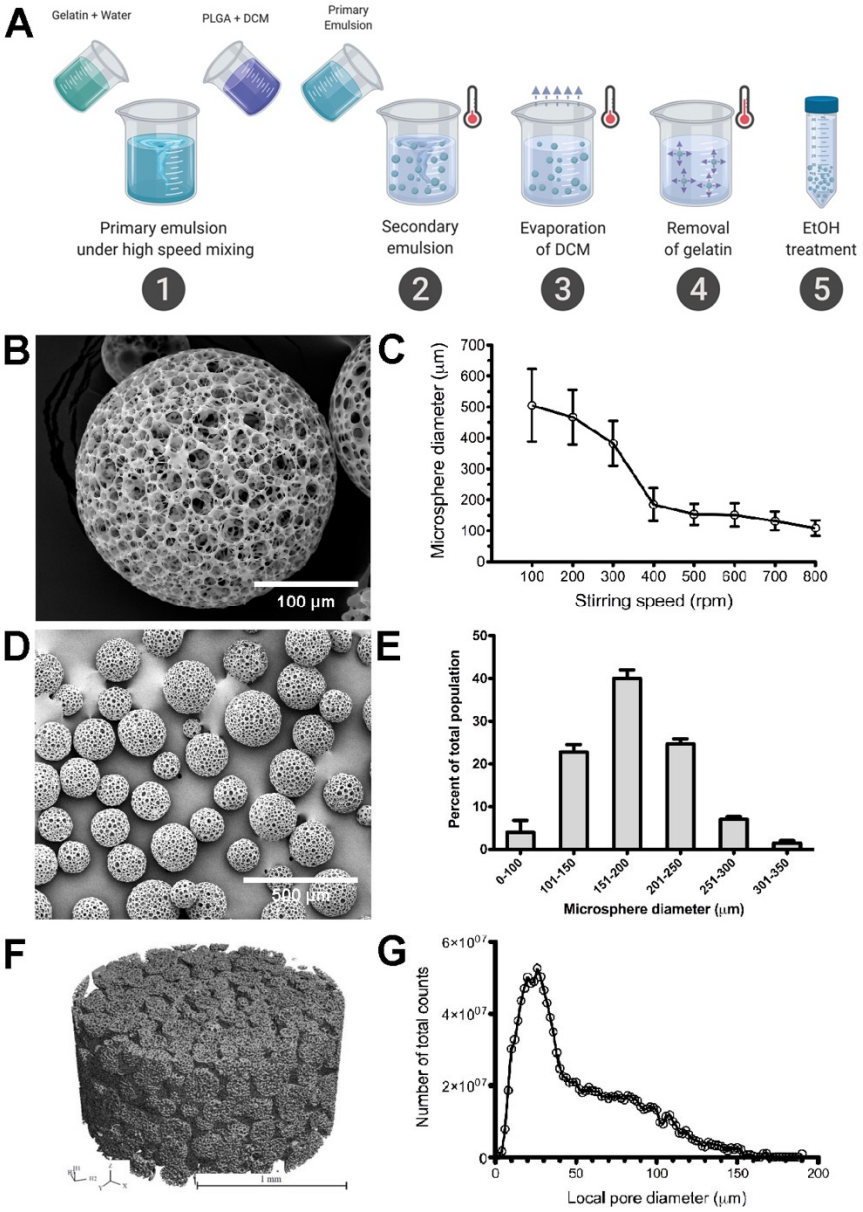

362

363 **Figure 1. Preparation and characterization of the microsphere scaffold.** (A) Illustration of the double
364 emulsion and porogen leaching process used to prepare porous PLGA microspheres; (B) SEM image of
365 a single porous microsphere (scale bar = 100 µm); (C) Defined stirring speed during secondary emulsion
366 dramatically impacted mean microsphere diameter. (n=3 per treatment, each group contained 250
367 microspheres); (D) SEM Image of a representative batch of microspheres (scale bar = 500 µm); (E)
368 Distribution of microsphere size across multiple batch preparations using a stirring speed of 400 rpm (n =
369 3 biological replicates, each replicate contained 250 microspheres); (F) Micro CT image of internal
370 microsphere structure (scale bar = 1 mm). (G) Local pore diameter as calculated by micro CT. Error bars
371 represent ± standard deviation.

microsphere assays. Microspheres were packed into a micro CT chamber with a volume of 3.14 mm^3 (**Figure 1F**). Analysis revealed a local pore diameter of 50 ± 35 μm, >88% porosity, and an open, interconnected pore structure (**Figure 1G**). The process described in this study optimizes the microsphere porosity, size distribution, and reproducibility for use as a scalable platform for 3D cell culture applications.

The mechanical properties of microsphere scaffolds are impacted by hydration

Nanoindentation assays were performed to determine the mechanical properties of PLGA samples. The nanomechanical properties of PLGA thin-film (dry state) and microspheres (both dry and hydrated states) were determined as a function of hydration (T_h). The load-displacement response for the PLGA thin-film and microspheres were measured in displacement-controlled loading and unloading mode. We determined the average elastic modulus (E) for non-hydrated PLGA thin-films of 3.3% (w/v), 5% (w/v), or 6.6% (w/v) was E = 1.48, 0.619, and 0.129 GPa, respectively. The indentation hardness (H_{IT}) obtained for these films equated to 34.6 ± 2.4 MPa, 15 ± 1.1 MPa, and 6.2 ± 0.4 MPa for 3.3% (w/v), 5% (w/v), and 6.6% (w/v) non-hydrated PLGA films, respectively. By comparison, the elastic modulus and indentation hardness values for non-hydrated PLGA microspheres (3.3% (w/v)) were significantly lower (E = 76.6 ± 10 MPa and H_{IT} = 5.4 ± 0.5 MPa, respectively) than non-hydrated thin-film (3.3% (w/v)), demonstrating the mechanical impact of porous architecture (**Figure 2A**). The force-displacement response from PLGA microsphere indentation captures both the microstructural response of the PLGA polymer structure as well as the pore spaces. The highly porous microspheres produced significantly lower mechanical properties compared to the film. The elastic modulus and indentation hardness of the PLGA microspheres (3.3% (w/v)) decreased as hydration increased (**Figure 2B, C**). For hydrated microspheres, a nearly 40% decrease in modulus (**Figure 2B**) was observed after 24 h hydration relative to the dry state (E = 76.6 ± 10 MPa). The modulus dropped to E = 29.3 ± 2.8 MPa, 24.9 ± 1.3 MPa and 14.9 ± 1.5 MPa on d1, d2, and d7, respectively. The hardness values also decreased similarly with increased hydration (**Figure 2C**). While H_{IT} = 5.4 ± 0.5 MPa in the dry state, H_{IT} decreased over time with prolonged hydration (H_{IT} = 2.4 ± 0.3 MPa, 1.7 ± 0.1 MPa and 1.44 ± 0.2 MPa on d1, d2 and d7, respectively). These data demonstrate our PLGA-based scaffold exhibits mechanical properties that become more tissue-like with incubation in aqueous solutions such as culture media.

Optimization of iPSC-derived NSC scaffold attachment

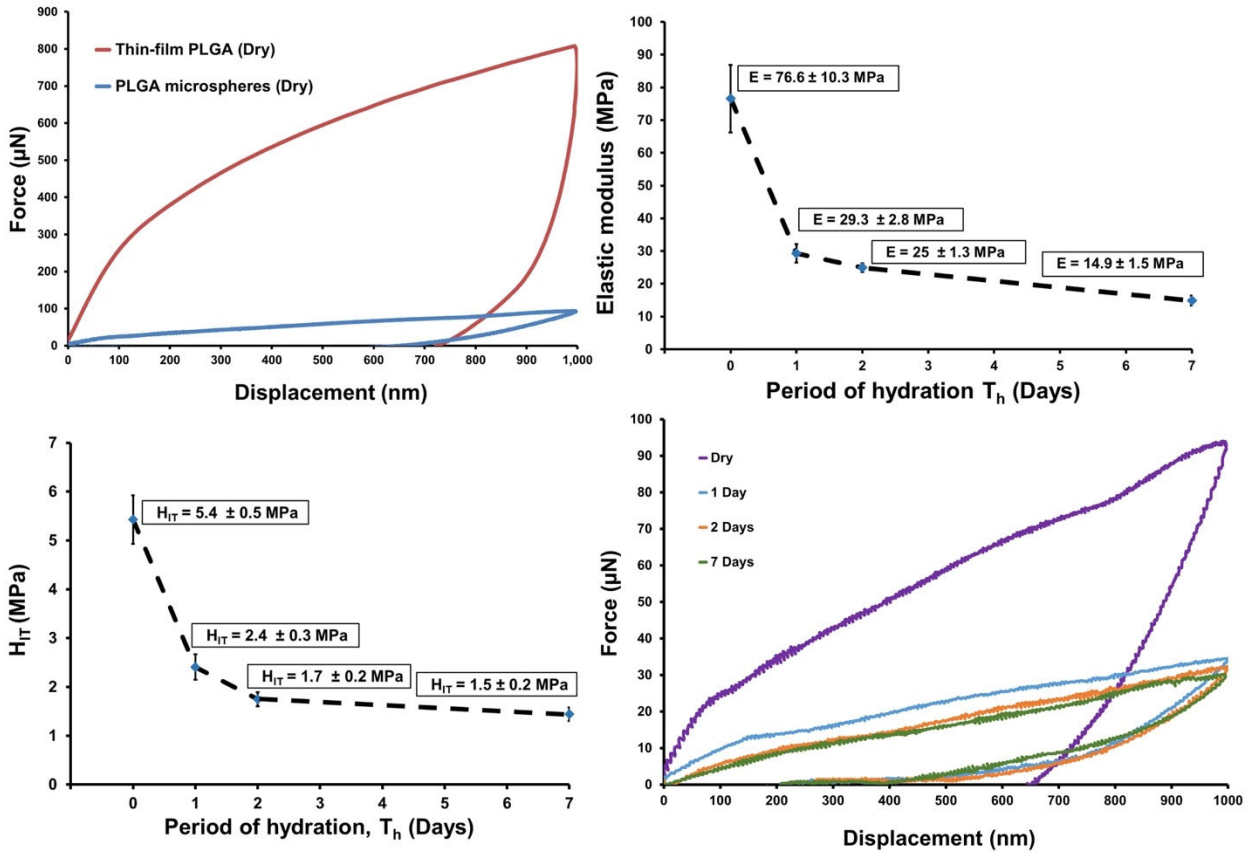

403

404 **Figure 2. Hydration of the microsphere scaffold (3.3% (w/v)) shifts load-displacement curves, the**
405 **elastic modulus, and indentation hardness as a function of time.** (A) Load-displacement response for
406 the PLGA thin-film and microspheres in a dry state demonstrates the softening effect of the porous
407 microstructure of microspheres. (B), (C), (D) Deformation response and mechanical properties of the
408 hydrated PLGA microspheres compared to the dry state with degradation. All error bars for elastic modulus
409 measurements (panel B) and indentation hardness (panel C) are represented as ± standard deviation.

410

411

412

413

414

415

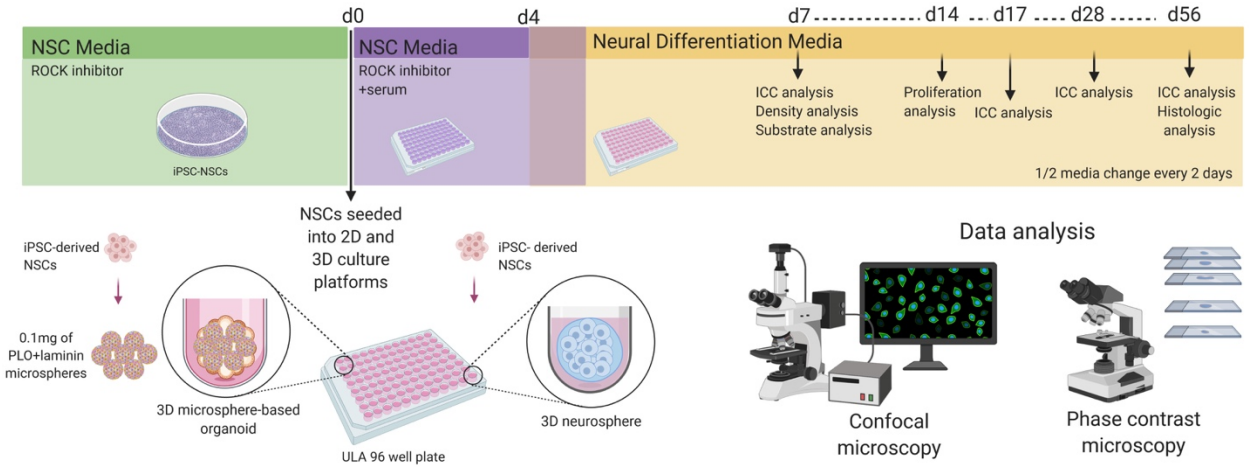

Figure 3. Assay schema for validating the use of a PLGA-based microsphere system for neural cell models. iPSC-derived NSCs were either cultured in traditional 2D systems, grown as self-aggregating 3D neurospheres, or seeded onto 3D microsphere based structures. Cultures were then analyzed for various cellular parameters including attachment, proliferation, differentiation, and co-culture.

We next sought to determine whether our newly developed PLGA-based material could function as a cellular scaffold and model for neurodevelopment. Beginning with the addition of iPSC-derived NSCs to the scaffold, we outlined a series of assays to qualify the ability of our PLGA-based material to promote NSC attachment, proliferation, differentiation, and support co-culture studies (**Figure 3**). To first determine the efficiency of iPSC-derived NSC attachment onto our PLGA microsphere surface, NSCs were cultured with unmodified PLGA microspheres in the presence or absence of FBS for 1, 3, 5, or 7 days (**Figure 4A**). The addition of serum has previously been shown to aid in the attachment of neural cell types to culture matrices.[43-47] Through balancing the positive impact on NSC attachment while minimizing the influence of FBS on neural differentiation, neural differentiation and tissue modeling could be optimized. NSCs were passively seeded onto unmodified PLGA microspheres in the presence or absence of FBS and cultured for 7 days before being fixed for immunocytochemistry (ICC) (**Figure 4A**). Analysis of two distinct NSC lines revealed that serum supplementation for any length of time increased the number of nuclei per microsphere compared to non-FBS supplemented (**Figure 4B,C**). Additionally, F-actin expression, as a measure of cytoskeleton formation, was increased by NSC serum supplementation (**Figure 4D**). While these data suggest short-term exposure to serum increases NSC microsphere attachment, substrates which avoid the inhibitory effects of serum on neural differentiation may benefit NSC properties.[48]

Through serum-free culture of embryoid body-like aggregates with quick reaggregation (SFEBq), *in vitro* neuronal differentiation can be achieved in the absence of extrinsic neural induction factors.[3, 18, 49, 50] It is also established that growth factor and protein-rich hydrogels such as Matrigel support the development of 3D neural cultures.[51] Since our biomaterial-based methodology supports 3D self-organization and the minimization of undefined factors, we compared the responses of NSCs cultured on uncoated microspheres to microspheres coated with two different neural supportive substrates: PLO+laminin and Matrigel. Confocal microscopy images demonstrated NSCs attached to either uncoated, PLO+laminin-coated, or Matrigel-coated microspheres (**Figure 5A**). NSCs demonstrated an increase in cell number over the measured time course across all conditions (**Figure 5B**). Calculations of F-Actin produced per cell showed a relatively consistent trend over the time course (**Figure 5C**).[52] While NSCs exhibited 60-70% positivity for the proliferation marker Ki67 across all culture conditions early on (**Figure 5D**), a universal reduction in $Ki67^{+}$ cells was subsequently observed across all conditions, suggesting terminal differentiation has likely begun (**Figure 5D**). These results are consistent with previous *in vitro* 3D culture models demonstrating a reduction in Ki67 expression in the early stages of differentiation.[53] Our data demonstrate that cells cultured on uncoated or PLO+laminin coated

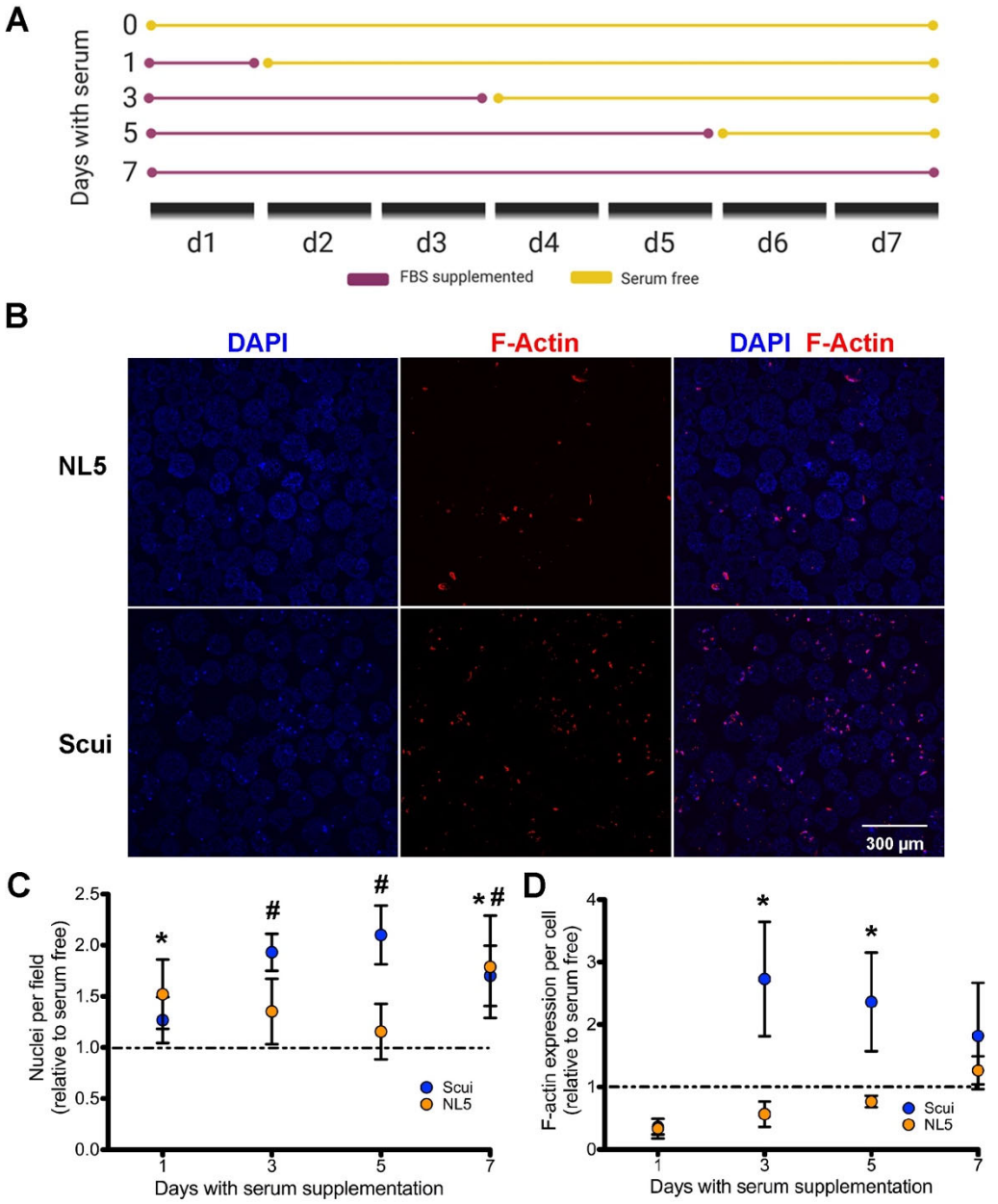

468

469 **Figure 4. Serum improves attachment and cytoskeleton production by microsphere-cultured**
470 **NSCs.** (A) Diagram depicting the experimental design for serum supplemented media exposure. (B)
471 Confocal images of NSCs on uncoated microspheres after 7 days of serum supplementation; nuclei
472 identified with DAPI and F-actin filaments labeled with Phalloidin Texas-red (scale bar = 300 µm). (C)
473 Nuclei counts of NSCs after varying duration of serum supplementation; n = 3 biological replicates per
474 group. (D) Quantified F-actin per cell by Phalloidin Texas-red after varying durations of serum
475 supplementation; n = 3 biological replicates per group. Error bars represent ± standard deviation. *
476 indicates significant increase ($p < 0.05$) in Scui NSCs compared to serum-free control; # indicates
477 significant increase ($p < 0.05$) in NL5 NSCs compared to serum-free control.

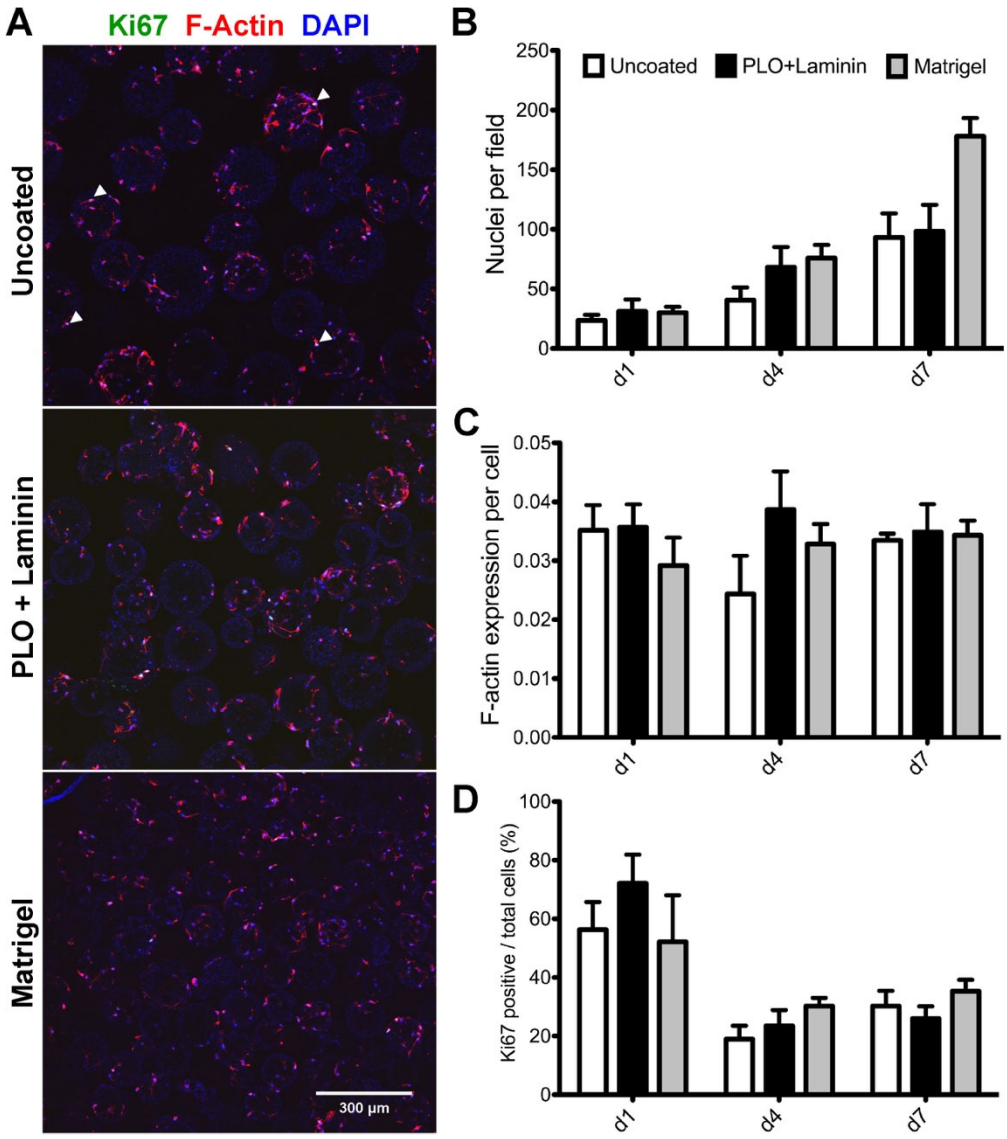

Figure 5. Neural supportive substrates promote proliferation and cytoskeletal production from microsphere-cultured NSCs. (A) Confocal images of Scui NSCs at d7 on uncoated microspheres (top panel), PLO+laminin coated microspheres (middle panel), and Matrigel coated microspheres (bottom panel) (scale bar = 200 µm). Arrowheads indicate selected Ki67 positive cells. (B) Increasing cell counts on uncoated, PLO+laminin-coated, and Matrigel-coated microspheres over 7 days. (C) The volume of F-actin per cell on d7 remained constant despite increasing cell number. (D) No significant difference in the percentage of Ki67 positive cells was observed between uncoated and coated microspheres. n = 15 (3 biological replicates and 5 image fields per group). Error bars represent ± standard deviation.

microsphere scaffolds display comparable characteristics to those exposed to the poorly defined supportive effects of Matrigel.

A scaffold-based model supports neural differentiation of both control and patient-derived iPSC models

Recent studies have questioned the quality of 2D monolayer neural culture due to the inability of cells to become polarized on rigid, flat surfaces.[19, 54] To evaluate the differentiation of iPSC-derived NSCs cultured on a microsphere scaffold to traditional differentiation models, we compared the differentiation of control and patient-derived iPSCs within a two-dimensional system, as self-aggregating neurospheres, and cultured on microsphere scaffolds. The CWI 4F2 patient iPSC line is a model for the cholesterol synthesis disorder Smith-Lemli-Opitz syndrome, a rare disease where subjects exhibit significant neurological malformations.[41, 55] We previously demonstrated this cell line exhibits stem cell defects and accelerated neuronal differentiation.[41] After 7 days of differentiation, we verified the multilineage differentiation of both control and patient-derived NSCs using immunocytochemistry. Cultured cell lines exhibited extensive expression of the human neural progenitor marker hNestin, pan-neuronal marker βIII-tubulin, the neuronal dendritic marker microtubule associated protein-2 (MAP2), and the astrocyte marker glial fibrillary acidic protein (GFAP) (**Figure 6A-C**). Compared to traditional two-dimensional culture, spheroid culture allowed for abundant hNestin+ neural progenitors but very little NF-M expression (**Figure 6D,E**). In scaffold-based culture, control (NL5) NSCs showed abundant hNestin expression, F-Actin and high expression of NF-M (**Figure 6F,G**). Patient (CWI 4F2) neurospheres exhibited both high levels of Sox2 and NF-M compared to NL5, in agreement with the previously published accelerated neuronal differentiation phenotype in this model (**Figure 6H,I**).[41] In comparison, CWI 4F2 cultured scaffolds demonstrated a mixed neural lineage, including $Sox2^+$ and $hNestin^+$ NSCs, as well as extensive NF-M expression (**Figure 6J,K**). Analysis of F-actin also demonstrated increased cytoskeleton formation within both control and patient-derived cells on scaffold vs. neurospheres (**Figure 6D,F,H,J**).

After 28 days of differentiation, NSCs cultured on two-dimensional PLO+laminin coated coverslips underwent considerable morphological change. While extensive $GFAP^+$ astrocytes were observed by d28, differentiated neurons formed cell clumps and demonstrated loss of cell adhesion associated with diminished cell health (**Figure 7A,B**). While spheroid cultures maintained a uniform cell distribution and overall structure, spheroid size was unchanged compared to d7. Further, spheroids exhibited increased $NF\text{-}M^+$ neurons compared to d7 while maintaining high F-Actin and hNestin levels (**Figure 7C,D**). However, GFAP expression was not

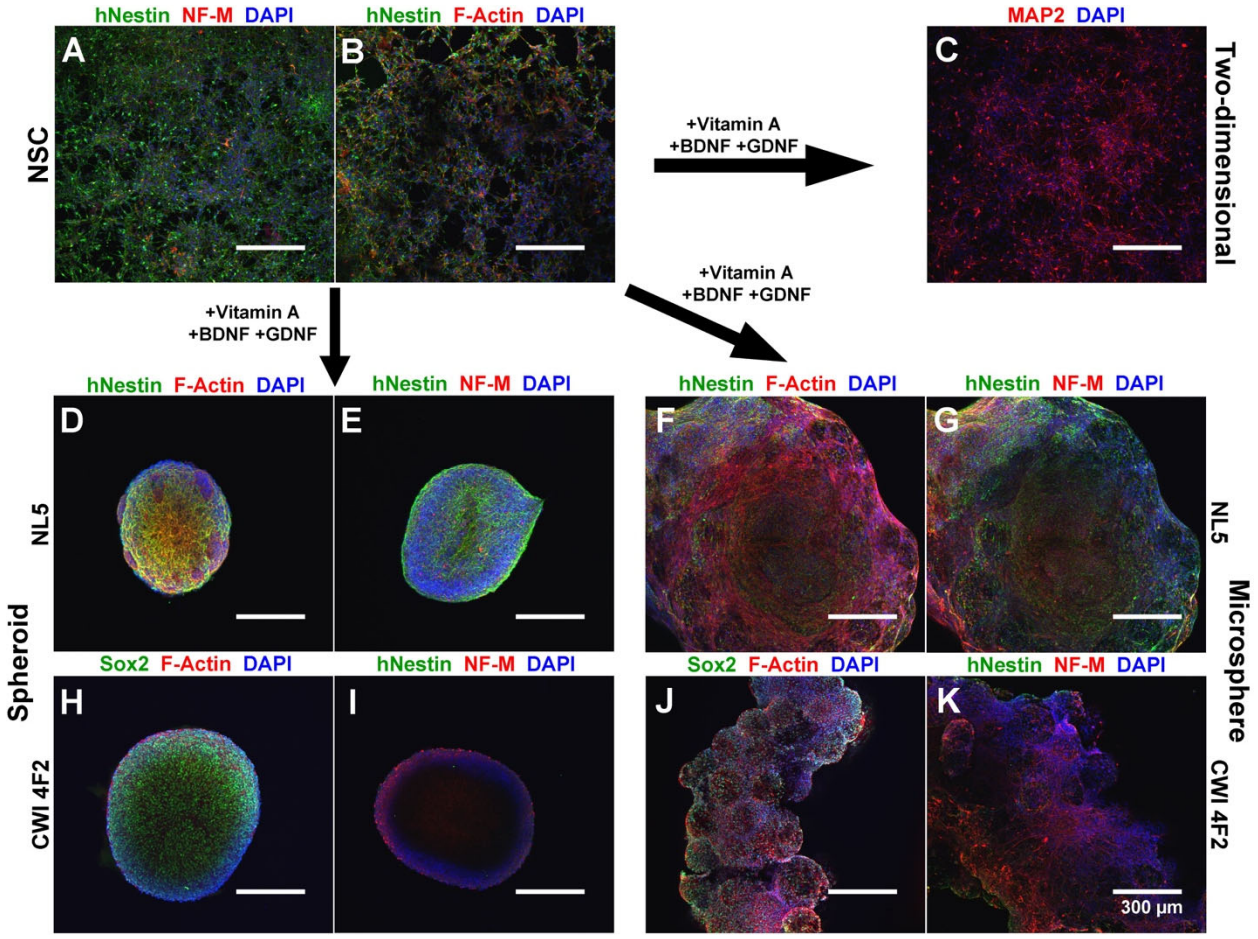

Figure 6. Microsphere-cultured control and patient-derived iPSC derivatives exhibit early neuronal lineage commitment. Comparison of control (NL5) and patient (CWI 4F2) models in 2D, 3D neurospheres, and 3D microspheres after 7 days differentiation. (A,B) NSCs exhibit low amounts of NF-M and F-Actin, but abundant hNestin expression. (C) 2D differentiation produces extensive MAP2 expression. (D,E) Control NSCs cultured as scaffold-free neurospheres labeled by ICC for hNestin, F-Actin, and DAPI (D) or hNestin, NF-M, and DAPI (E). (F,G) Control NSCs cultured as cellular scaffolds labeled by ICC for hNestin, F-Actin, and DAPI (F) or hNestin, NF-M, and DAPI (G). (H,I) CWI 4F2 NSCs cultured as a scaffold-free neurosphere labeled by ICC for Sox2, F-Actin, and DAPI (H) or hNestin, NF-M, and DAPI (I). (J,K) CWI 4F2 NSC scaffolds labeled by ICC for Sox2, F-Actin, and DAPI (J) or hNestin, NF-M, and DAPI (K) (scale bar = 300 µm).

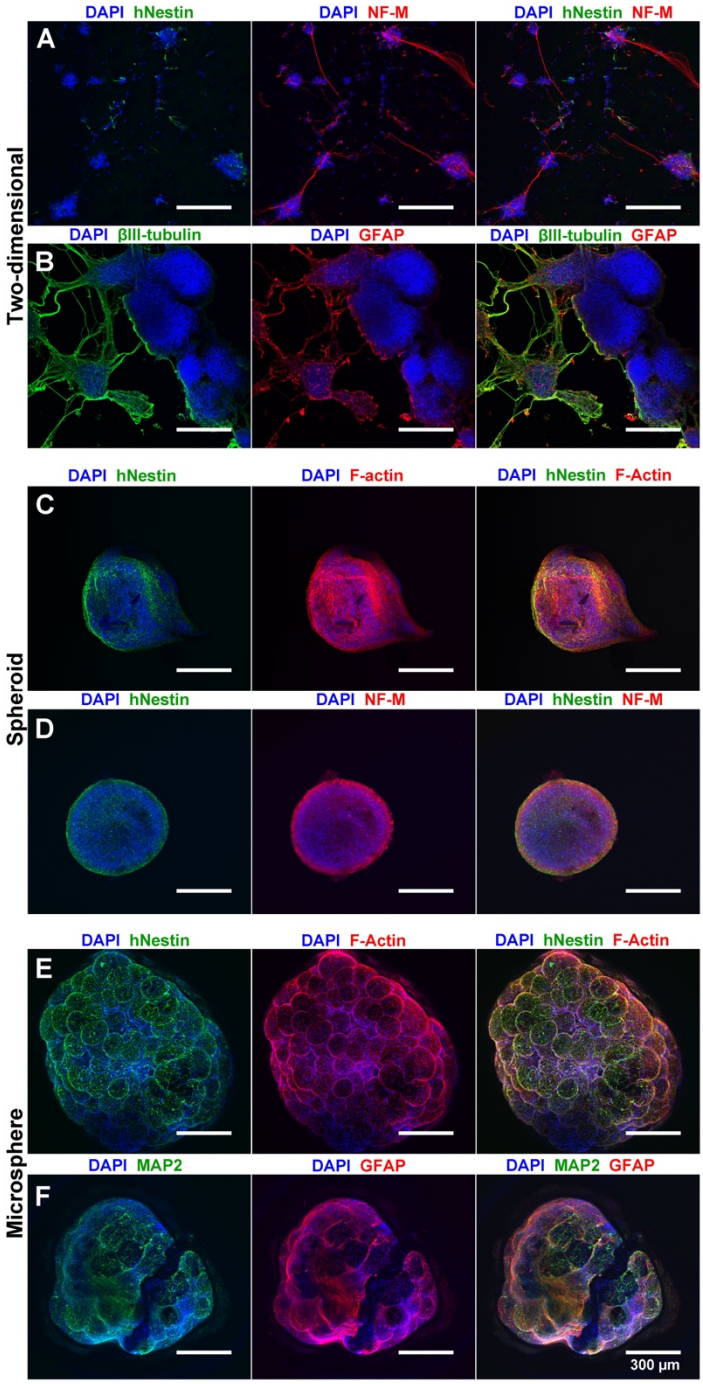

Figure 7. Microsphere culture allows NSC differentiation to neuronal and glial lineages. (A,B) 28 day differentiation in 2D conditions generates extensive neuronal (NF-M, βIII-tubulin) and astrocyte (GFAP) formation with loss of NSCs (hNestin) (DAPI nuclear counterstain). (C,D) Spheroid culture maintains NSCs (hNestin) over 28 days with neuronal (NF-M) and cytoskeletal (F-actin) formation. (DAPI nuclear counterstain). (E,F) Microsphere culture allows for expansion and cytoskeletal production of NSCs (hNestin, F-actin), as well as robust differentiation to neuronal (MAP2) and astrocytic (GFAP) lineages. (scale bar = 300 µm).

observed in spheroids. In comparison to spheroid cultures, the diameter of microsphere scaffold cultures was significantly increased on d28 of differentiation (**Figure 7E,F**). Scaffold-based cultures also demonstrated extensive glial differentiation, as exhibited by $GFAP^+$ cell types. Expansive glial differentiation within scaffold-based cultures was not at the expense of neuronal differentiation, as evidenced by extensive MAP2 expression. Using immunohistochemistry, we further determined that scaffold-based cultures exhibited integration of NSC-derived cells throughout the microsphere (**Supplemental Figure 2**). H&E staining demonstrated broad distribution of cells throughout the scaffold, validating the ability of cells to migrate from the scaffold's exterior surface. Overall, these assays demonstrate that our microsphere matrix provided a chemically defined, neural-supportive microenvironment which allows expansion, migration and multilineage differentiation of both control and patient-derived NSCs.

Recent work has demonstrated co-culture of endothelial cells with iPSC-derived models supports neural health and maturation.[56, 57] To demonstrate the capacity of our scaffold-based system for multi-lineage co-culture, NSCs, astrocytes, and endothelial cells were sequentially seeded onto a PLO+laminin coated microsphere scaffold. NSCs were first seeded onto microspheres in ultra-low attachment 96 well plates, followed by astrocytes and finally HUVECs (**Figure 8A**). As demonstrated by expression of βIII-tubulin, GFAP, and CD31 on d7 of co-culture, the scaffold allows for attachment, survival, and integration of each cell type (**Figure 8**). F-actin expression, identified by Phalloidin Texas-red, and nuclear counterstaining demonstrate broad cell distribution and cytoskeletal formation throughout the microsphere-based scaffold (**Figure 8L,O**). ICC demonstrated that astrocytes, neurons, and HUVECs were still identifiable within the cellular scaffold on d28 of co-culture (**Figure 8F,K,P**). Increased expression of NF-M, GFAP and CD31 on d28 suggests increased neuronal maturation and proliferation of astrocytes and HUVECs (**Figure 8F,K,P**). Further, maintenance of hNestin+ cells at d28 suggests continued NSC maintenance within this co-culture scaffold. These data further demonstrate the ability of the microsphere scaffold for robust co-culture of neural, glial, and endothelial cells, representing a critical initial step towards the formation of mature, nutrient-rich, and vascularized 3D structures using this material[58].

Microspheres can function as a platform for sustained growth factor release

Neural differentiation of iPSCs requires frequent exogenous supplementation of defined cocktails of growth factors and cytokines to promote cell proliferation, differentiation, and tissue organization. To determine if microspheres could function in both cellular support and growth

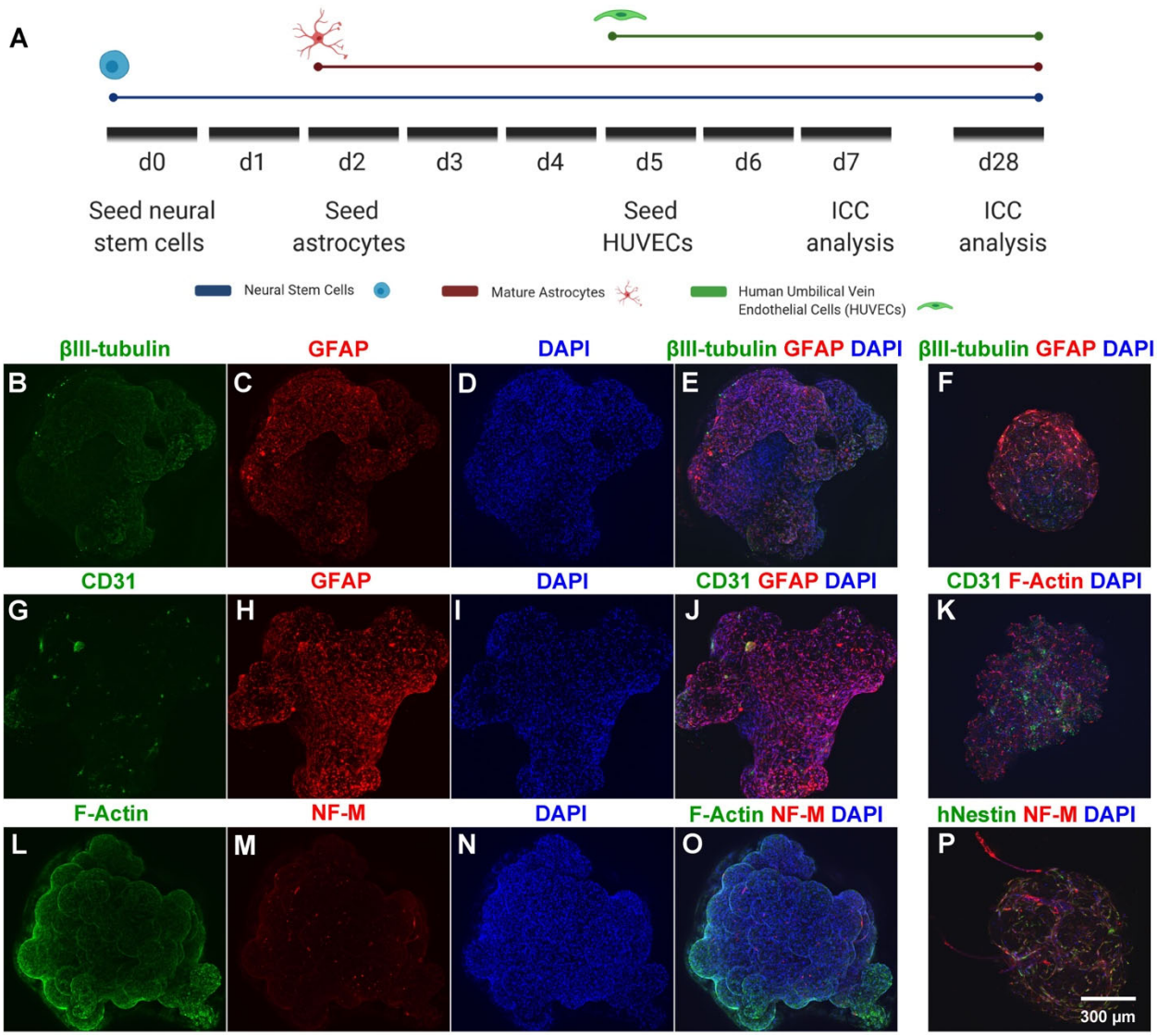

Figure 8. Microsphere-based scaffolds support the co-culture of NSCs, astrocytes, and HUVECs. (A) Cell seeding and ICC analysis timeline. Confocal images displayed as maximum projections of iPSC-derived NSCs, astrocytes, and HUVECs within scaffold. (B-E) d7 ICC for neurons (βIII-tubulin) and astrocytes (GFAP). (F) d28 ICC for neurons (βIII-tubulin) and astrocytes (GFAP). (G-J) d7 ICC for HUVECs (CD31) and astrocytes (GFAP). (K) d28 ICC for HUVECs (CD31) and cytoskeletal formation (F-actin). (L-O) d7 ICC for cytoskeletal formation (F-actin) and mature neurons (NF-M). (P) d28 ICC for neural progenitors (hNestin) and mature neurons (NF-M). DAPI nuclear counterstain is also shown. (Scale bar = 300 µm).

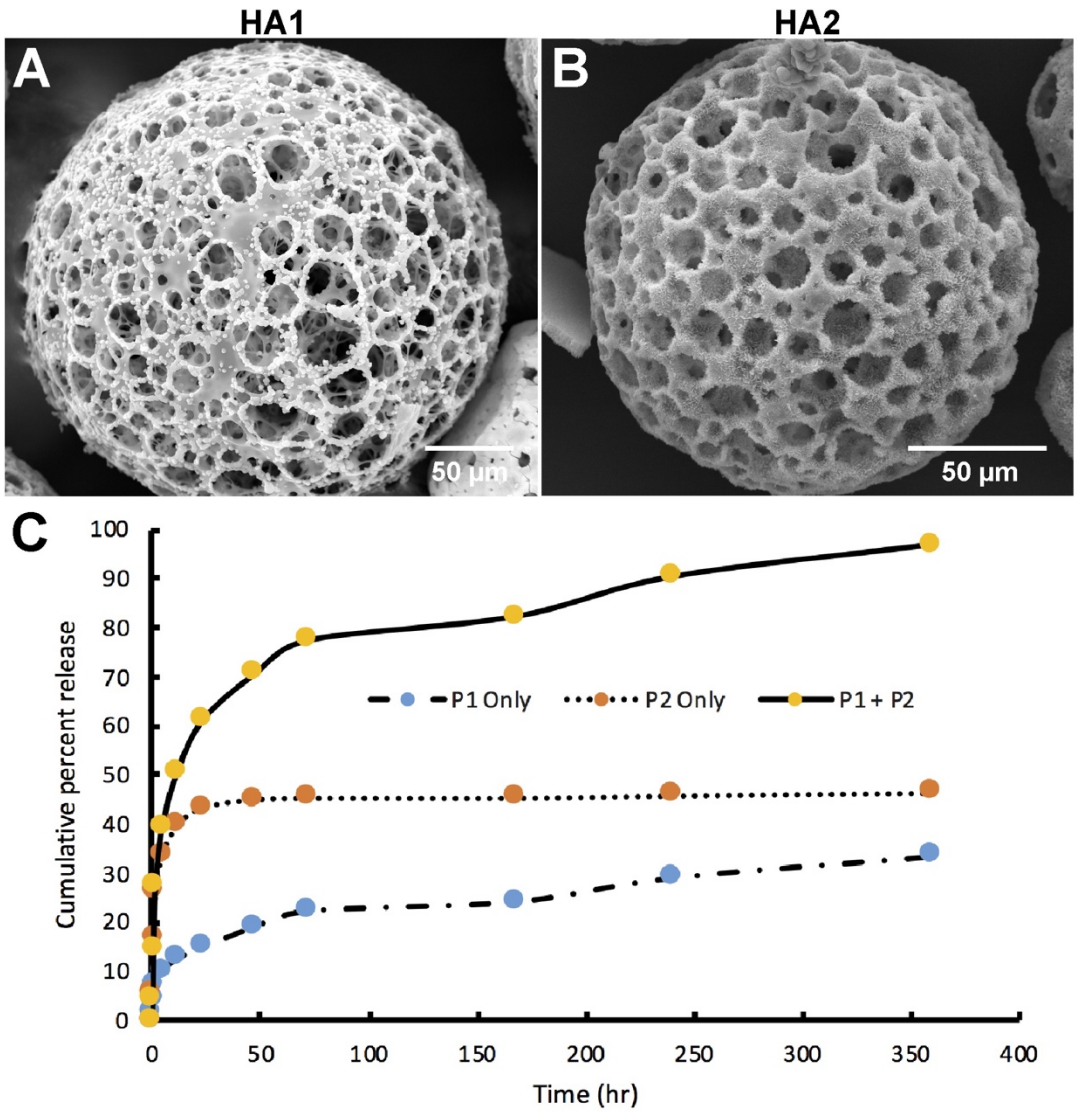

Figure 9. Hydroxyapatite coated microspheres allow for protein loading and release. (A) An SEM image of a PLGA microsphere covered in hydroxyapatite nucleation crystals after immersion in SBF phase I (P1) solution (scale bar = 50 µm). (B) An SEM image of a PLGA microsphere covered in mature hydroxyapatite crystals after immersion in SBF phase II (P2) solution (scale bar = 50 µm). (C) Greater amounts of BSA were released from P1+P2 compared to P1 only or P2 only after 360 h in solution (n = 4).

596 factor release, microspheres were layered with hydroxyapatite crystals via SBF. While
597 hydroxyapatite has traditionally been utilized for osteogenic differentiations[59-61] , recent work has
598 demonstrated hydroxyapatite also promotes neural differentiation and functional neuronal
599 development through enhanced Ca^{2+} signaling.[62, 63] HA was deposited onto the entire exposed
600 exterior and interior surfaces of the microsphere, allowing crystal deposition without pore
601 occlusion (**Figure 9A,B**). The first SBF phase deposited on the microsphere surface (HA1) acts
602 as a nucleation site, while second phase deposition creates an additional layer (HA2) (**Figure**
603 **9A,B**). To model the capacity of the two HA layers to entrap and release proteins, BSA was added
604 to SBF phase 1 and phase 2 solutions. BSA entrapment was evaluated in three different
605 combinations: BSA added to SBF phase I only (P1 only), BSA added to SBF phase 2 (P2 only),
606 or BSA added to both SBF phases (P1+P2). While P1 only incorporation of BSA was relatively
607 inefficient (7.2%), P2 only (34.5%) and P1+P2 (56.3%) demonstrated robust protein incorporation
608 into HA layers. BSA release following P1+P2 entrapment was also highly efficient (96.9 ± 3.56%)
609 (**Figure 9C**). The release rates among the three groups varied in relation to their incorporation
610 efficiency. The P1 only group (7.2% incorporation efficiency) had an overall release rate of 0.008
611 µg/min during the 360-hour release timeframe. The P2 only group (34.5% incorporation efficiency)
612 had an overall release rate of 0.04 µg/min over 360 hours and the P1+P2 group (56.3%
613 incorporation efficiency) had an overall release rate of 0.14 µg/min.

614 After verifying that an entrapped protein could be loaded and released in a controlled and
615 sustained manner, we sought to determine if the scaffold could support loading and release of
616 multiple molecules. Two biomolecules were loaded into hydroxyapatite-coated microspheres: a
617 FITC-conjugated peptide was loaded into phase 1 HA and AlexaFluor647-conjugated BSA was
618 incorporated into phase 2 HA. NSCs were seeded onto the scaffold following protein entrapment,
619 followed by imaging for FITC, AlexaFluor647, and DAPI counterstained NSC nuclei (**Figure 10A**).
620 NSCs attached onto the surfaces of all HA-coated microspheres and formed robust cytoskeletal
621 projections across the scaffold (**Figure 10B**). To determine the bioactivity of entrapped
622 biomolecules, bFGF was entrapped in both phases of the HA crystal matrix (P1+P2). The loading
623 of bFGF into both HA layers did not interfere with the porous structure of the microsphere, as the
624 microsphere matrix was covered in HA crystals (**Figure 10C**). While bFGF-loaded crystals
625 appeared somewhat flattened compared to HA crystals without loading (**Figure 10D**), the bFGF-
626 entrapped scaffold demonstrated increased NSC proliferation in scaffold cultures compared to
627 standard 2D culture (**Figure 10E**). These data demonstrate the microsphere scaffold can be
628 utilized for entrapment and release proteins of interest in a sustained manner, providing direct
629 trophic factor support to seeded cells.

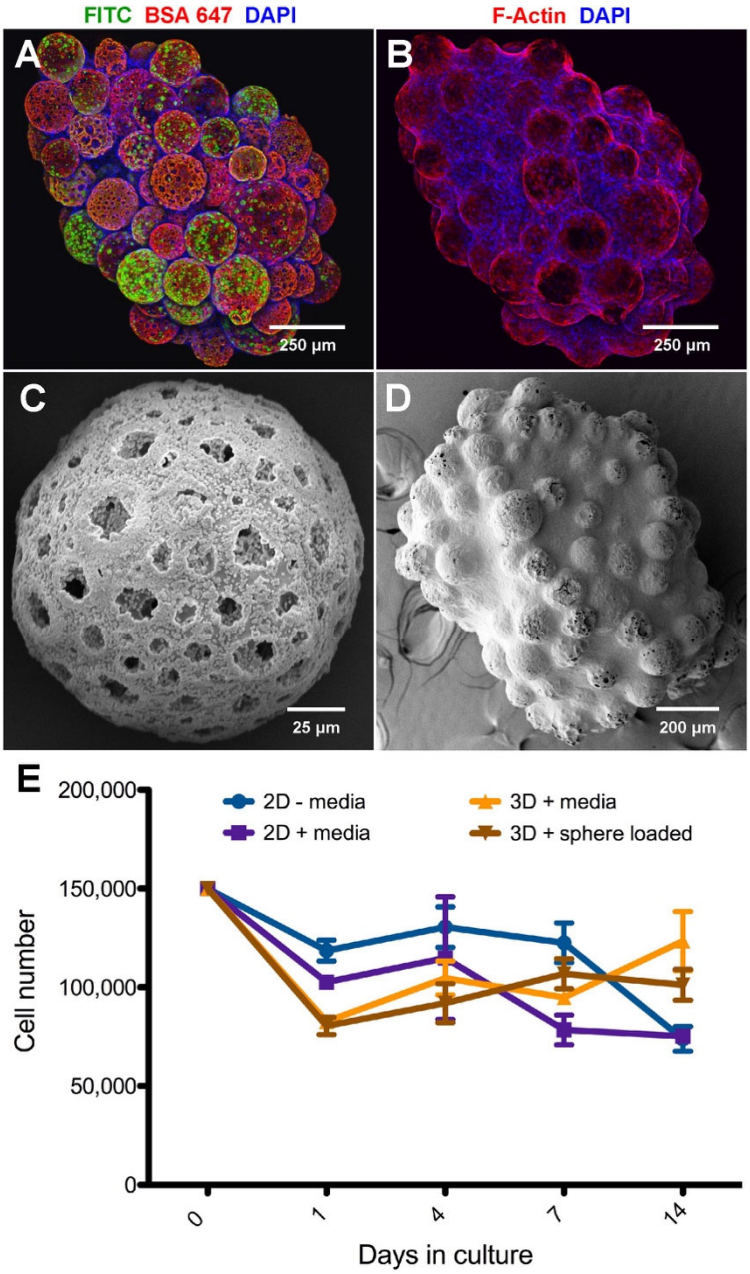

Figure 10. Protein-loaded and hydroxyapatite-coated microspheres supply growth factors directly to scaffold-cultured NSCs. (A) Confocal images of NSCs on an HA-microsphere-based scaffold with merged ICC channels showing FITC-peptide in phase I HA, BSA-AlexaFluor 647 in phase II HA, and cell nuclei counterstained with DAPI; scale bar = 250 µm. (B) Confocal images of NSCs on an HA-microsphere-based scaffold with merged ICC channels showing F-actin filaments identified with Phalloidin Texas-red and nuclei counterstained with DAPI; scale bar = 250 µm. C) SEM image of a microsphere with bFGF incorporated into HA matrix (+P1+P2) (scale bar = 25 µm); (D) SEM image of NSC cultured microsphere scaffold after 5 days. Scaffold contains bFGF incorporated into HA. (scale bar = 200 µm). (E) bFGF released directly from HA promoted NSC proliferation over 14 days comparably to bFGF-supplemented media. Error bars represent ± standard deviation.

Discussion

PLGA has been widely used as a biomaterial to support and direct cell fate through various 3D tissue engineering scaffold fabrication techniques such as electrospinning, soft lithography, gas foaming, particle leaching, supercritical CO_2, phase separation, 3D printing, and freeze-drying.[64-70] Polymeric and composite materials utilizing PLGA have been used to align tenocytes to support tendon repair, induce chondrogenesis of rabbit mesenchymal stem cells, promote hepatogenesis of human adipogenic stem cells, and differentiation of canine smooth muscles cells.[64, 66] PLGA scaffolds were used with and without the addition of transforming growth factor-β3 to support the delivery and differentiation of mesenchymal stem cells towards articular cartilage in vivo.[71] Our work has demonstrated PLGA microspheres provide a multifunctional, 3D cell culture platform also capable of loading and releasing proteins, peptides, and other growth factors. By incorporating biocompatible materials, using defined starting numbers of stem cells, and providing a chemically defined environment, our scaffold platform addresses some of the current challenges limiting the utility of 3D cell culture.[15] The microsphere scaffold developed here can be readily produced in high numbers, the product is shelf-stable for future use, and the final microsphere diameter is tunable during preparation. We have further demonstrated this system can be used to allow effective neural differentiation in three dimensions. Though Young's modulus of PLGA is higher than the presumptive ECM of the brain, substrate stiffness differs between areas of the brain and within glial subtypes. Studies have reported a stiffness range from 0.1 to 16 kPa across brain regions.[1, 11, 72] Substrate stiffness also influences neural subtype differentiation. Neuronal differentiation favors softer substrates (100-500 Pa) while stiffer substrates (1-10 kPa) favor glial differentiation.[1, 72] Rat NPCs cultured on surfaces with stiffness up to 35 kPa were not affected by the discrepancy to native tissue stiffness.[1] Despite having a higher elastic modulus in its dry state, PLGA undergoes bulk degradation through hydrolytic cleavage of ester bonds along the polymer backbone as water penetrates the matrix.[73, 74] As our work confirms, PLGA was previously shown to soften over the first 48 h due to a 221- 350% increase in water content. [74, 75] Previous work with PLGA has demonstrated a significant reduction of the elastic modulus due to matrix swelling and rapid loss of molecular weight through the bulk degradation process.[73, 75] In our study, hydration of PLGA microspheres reduced the elastic modulus by approximately four-fold. The microspheres used here were designed to be a malleable substrate that softens and degrades, allowing for cell remodeling and migration.[16]

The undefined ECM and growth factor milieu of naturally-derived hydrogels exposes self-aggregating and self-organizing cells to a poorly controlled mix of excitatory, proliferative, instructive, mechanotransducive, and inhibitory signals.[16, 51, 76] Matrigel-based methods can result in low reproducibility and poor control of differentiation due to the inherent variability within Matrigel.[4, 77] The use of a chemically undefined environments may also obscure or limit the utility of observations.[4, 16, 18, 72, 78, 79] The use of serum-free formulations has created more defined and consistent neural differentiation methods.[10, 80, 81] Therefore, a more defined 3D structure which incorporates neural ECM components would be a beneficial differentiation platform. Through incorporation of substrate-specific matrices such as PLO+laminin, this study offers improved control over the *in vitro* microenvironment by providing physiologically relevant cues found in the brain.[1, 10, 66, 76, 82, 83] We have demonstrated microspheres promote iPSC-derived NSC growth and differentiation. Compared to cell-only 3D neurospheres, which rely on cell aggregation, cell-secreted ECM proteins, and self-organization to generate the 3D structure, the microspheres can be coated with ECM proteins and ligands to mechanically and chemically direct stem cell differentiation. Scaffolds with high porosity and nearly 100% interconnected pore structure, such as the microsphere platform presented here, allow for nutrients, oxygen, and waste products to be transported throughout the biomaterial-based organoid structure.[1, 84] We have modeled the flow of solution through the microsphere by the deposition of HA crystals throughout the internal architecture of the microsphere. The larger surface area, porosity, and biocompatibility of PLGA microspheres support cell attachment, growth and differentiation.[4, 32, 85] The acidic by-products that form upon matrix degradation can lower the pH and lead to inflammation within PLGA-based scaffolds.[74, 86, 87] However, less than 12% of our microsphere volume is composed of PLGA. Further, the interconnected pore structure allows lactic acid and glycolic acid monomers to be diluted within the surrounding media, limiting toxicity on scaffold-based cells.[64, 66, 87] Lastly, the porous matrix and the high surface area of the scaffolds create a supportive environment that promote cellular health and complexity compared to cell-based neurospheres.

Due to the frequent inability of animal models to recapitulate disease manifestation,[1, 14, 88] the ability to model human disease using iPSCs in a 3D environment is critical for both basic and translational research. The ability to model human disease *in vitro* with iPSCs allows access to both unaffected and disease-impacted cell types of interest, providing opportunities for analysis of disease pathogenesis or drug discovery studies.[2] However, the cellular complexity of iPSC-based neurological models has been limited due to the stochastic nature of the differentiation process. We have demonstrated that our 3D microsphere-based scaffold system can function as

an *in vitro* neurodevelopment platform using iPSC-derived cells. Our system can support both unaffected and disease-affected iPSC models, as well as combinatorial culture of progenitors, differentiated neuronal and glial cell types, and endothelium.[1, 6, 27, 50, 88 41]

While we have demonstrated our microsphere platform can successfully host cell types of interest, future studies utilizing this platform will determine the functional activity of cultured cells, the impact of cell-to-cell interactions, optimization of cell populations, and utilization of ECM coatings favorable to specific cell types. Such studies will involve prolonged, multi-month culture to allow maturation and functional development of cellular networks as has previously been performed in self-organizing cerebral organoid models.[17, 89] Through directed differentiation towards specific cell types of interest on separate scaffolds, the microspheres could be combined, similar to assembloids, to create composite scaffolds with greater heterogeneity and functionality.[90, 91] The microsphere-based scaffold architecture offers a unique platform to assemble distinct clusters of differentiating cells to maximize recapitulation of CNS regions of interest. Future studies will therefore be needed to determine the precise impact of our microsphere scaffold on the formation and function of defined neuronal and glial populations.

Our data demonstrates the microsphere platform described can function as both a cellular scaffold and growth factor elution system consisting of biocompatible materials. This work provides important proof-of-concept data regarding the multifunctionality of this system. The HA coated microspheres described here can be loaded with multiple growth factors, as demonstrated by incorporation of two fluorescently bound molecules. Future work will evaluate other bioactive molecules, such as silk nanofibers, which limit substrate stiffness compared to HA for the incorporation and release of soluble factors.[92] The incorporation of physiologically critical growth factors, such as bFGF, into a 3D platform has the capacity to promote progenitor proliferation or drive cellular differentiation without additional environmental manipulation. Proteins, peptides and other small molecules can thus be released directly to cells to modify a signaling pathway or cellular function without disturbing the growing organoid. The porous structure allows for a much greater loading capacity due to the surface area, as well as the rapid clearance of any acidic by-products that may interfere with the bioactivity of sensitive molecules.[74] We demonstrated that bFGF, released from microspheres over 14 days, increased proliferation above the level of the 2D monolayer which was receiving bFGF supplemented media every other day. In a similar manner to coating microspheres with various proteins to model different ECM substrates, the microspheres can be dual loaded with factors to influence attached cells. For example, the

addition of a bioceramic component to PLGA microspheres is applicable for use in other, non-neural tissue engineering models.

In summary, we have developed a chemically-defined, microsphere-based cell culture platform to model neurodevelopment and disease pathogenesis using iPSC derivatives. The microspheres developed in this study represent a biodegradable, highly porous, customizable substrate capable of hosting NSCs and differentiated cells types for weeks *in vitro*. We show that the platform can be customized with various extracellular matrices such as PLO and laminin to support proliferation or directed differentiation, as desired. We further demonstrate these microspheres can support multiple neural and non-neural cell types simultaneously, through co-culture of NSCs, NSC-differentiated neurons, mature astrocytes, and HUVEC cells. Lastly, modified microspheres can simultaneously function as both a cellular scaffold and small molecule delivery platform. Future work will utilize the biophysical and nanoarchitectonic cues utilized here to generate complex culture systems for the study of development, disease pathogenesis, or 3D-based drug discovery assays.

Acknowledgements

We would like to thank the University of South Dakota Center for Brain and Behavior Research and the University of South Dakota Neuroscience, Nanotechnology, and Networks programs for their support. We would like to thank Kelly Graber and Claire Evans for assistance with H&E immunohistochemistry. The graphical abstract was created using BioRender.com.

Author contributions

ES, HS, and KRF conceived the study. ES performed most of the experiments under the supervision of DE and KRF. SVJ performed analysis of scaffold mechanical properties under the supervision of DRK and KSK. ES and KRF wrote the manuscript. All authors discussed the results and approved the final manuscript.

Declaration of conflicting interests

The authors declare no potential conflicts of interest with respect to the research, authorship, and/or publication of this article.

Funding

This study was supported by NIH grants (NIGMS P20 GM103620 and P20 GM103548), the National Science Foundation (DGE-1633213), a National Science Foundation/EPSCoR Cooperative Agreement (IIA-1355423), a National Science Foundation/EPSCoR Cooperative Agreement (OIA-1946202), and the State of South Dakota. The content is solely the responsibility of the authors and does not necessarily represent the official views of the National Institutes of Health or the National Science Foundation.

ORCID iD for corresponding author

Kevin Francis, https://orcid.org/0000-0002-3636-7264

Statement of significance

In this study, highly porous PLGA microspheres were prepared using a double emulsion and porogen leaching technique. The resulting microspheres were used as a 3D platform to culture control and patient iPSC-derived neural stem cells as a model for neurodevelopment. The goal of this research was to demonstrate that protein-coated microspheres could serve as a suitable *in vitro* model for the developing brain. Through our *in vitro* biological results, we have shown that the porous PLGA microspheres developed herein can simultaneously support multilineage differentiation, co-culture of neural and non-neural lineages, and directly deliver small molecules to 3D neural models. This platform represents a significant step in creating more reproducible three-dimensional models for the *in vitro* study of human disease or for use in drug discovery assays.

Data availability statement

Datasets generated in this study are available from the corresponding author upon request.

References

1. Murphy AR, Laslett A, O'Brien CM, et al. Scaffolds for 3D in vitro culture of neural lineage cells. *Acta Biomater* 2017; 54: 1-20. 2017/03/06. DOI: 10.1016/j.actbio.2017.02.046.
2. Sloan SA, Andersen J, Pasca AM, et al. Generation and assembly of human brain region-specific three-dimensional cultures. *Nat Protoc* 2018; 13: 2062-2085. 2018/09/12. DOI: 10.1038/s41596-018-0032-7.
3. Chukwurah E, Osmundsen A, Davis SW, et al. All Together Now: Modeling the Interaction of Neural With Non-neural Systems Using Organoid Models. *Front Neurosci* 2019; 13: 582. 2019/07/12. DOI: 10.3389/fnins.2019.00582.
4. Poli D, Magliaro C and Ahluwalia A. Experimental and Computational Methods for the Study of Cerebral Organoids: A Review. *Front Neurosci* 2019; 13: 162. 2019/03/21. DOI: 10.3389/fnins.2019.00162.

5. Centeno EGZ, Cimarosti H and Bithell A. 2D versus 3D human induced pluripotent stem cell-derived cultures for neurodegenerative disease modelling. *Mol Neurodegener* 2018; 13: 27. 2018/05/24. DOI: 10.1186/s13024-018-0258-4.
6. Lage OM, Ramos MC, Calisto R, et al. Current Screening Methodologies in Drug Discovery for Selected Human Diseases. *Mar Drugs* 2018; 16 2018/08/17. DOI: 10.3390/md16080279.
7. Saxe JP, Wu H, Kelly TK, et al. A phenotypic small-molecule screen identifies an orphan ligand-receptor pair that regulates neural stem cell differentiation. *Chem Biol* 2007; 14: 1019-1030. 2007/09/22. DOI: 10.1016/j.chembiol.2007.07.016.
8. Zhao WN, Cheng C, Theriault KM, et al. A high-throughput screen for Wnt/β-catenin signaling pathway modulators in human iPSC-derived neural progenitors. *J Biomol Screen* 2012; 17: 1252-1263. 2012/08/28. DOI: 10.1177/1087057112456876.
9. Horvath P, Aulner N, Bickle M, et al. Screening out irrelevant cell-based models of disease. *Nat Rev Drug Discov* 2016; 15: 751-769. 2016/11/04. DOI: 10.1038/nrd.2016.175.
10. Chen AK, Reuveny S and Oh SK. Application of human mesenchymal and pluripotent stem cell microcarrier cultures in cellular therapy: achievements and future direction. *Biotechnol Adv* 2013; 31: 1032-1046. 2013/03/28. DOI: 10.1016/j.biotechadv.2013.03.006.
11. Shah SB and Singh A. Cellular self-assembly and biomaterials-based organoid models of development and diseases. *Acta Biomater* 2017; 53: 29-45. 2017/02/06. DOI: 10.1016/j.actbio.2017.01.075.
12. Koo B, Choi B, Park H, et al. Past, Present, and Future of Brain Organoid Technology. *Mol Cells* 2019; 42: 617-627. 2019/09/30. DOI: 10.14348/molcells.2019.0162.
13. Edmondson R, Broglie JJ, Adcock AF, et al. Three-dimensional cell culture systems and their applications in drug discovery and cell-based biosensors. *Assay Drug Dev Technol* 2014; 12: 207-218. 2014/05/17. DOI: 10.1089/adt.2014.573.
14. Wang H. Modeling Neurological Diseases With Human Brain Organoids. *Front Synaptic Neurosci* 2018; 10: 15. 2018/06/26. DOI: 10.3389/fnsyn.2018.00015.
15. Amin ND and Pasca SP. Building Models of Brain Disorders with Three-Dimensional Organoids. *Neuron* 2018; 100: 389-405. 2018/10/26. DOI: 10.1016/j.neuron.2018.10.007.
16. Yin X, Mead BE, Safaee H, et al. Engineering Stem Cell Organoids. *Cell Stem Cell* 2016; 18: 25-38. 2016/01/11. DOI: 10.1016/j.stem.2015.12.005.
17. Lancaster MA and Knoblich JA. Generation of cerebral organoids from human pluripotent stem cells. *Nat Protoc* 2014; 9: 2329-2340. DOI: 10.1038/nprot.2014.158.
18. Lee CT, Bendriem RM, Wu WW, et al. 3D brain Organoids derived from pluripotent stem cells: promising experimental models for brain development and neurodegenerative disorders. *J Biomed Sci* 2017; 24: 59. 2017/08/22. DOI: 10.1186/s12929-017-0362-8.
19. Logan S, Arzua T, Canfield SG, et al. Studying Human Neurological Disorders Using Induced Pluripotent Stem Cells: From 2D Monolayer to 3D Organoid and Blood Brain Barrier Models. *Compr Physiol* 2019; 9: 565-611. 2019/03/16. DOI: 10.1002/cphy.c180025.
20. Kim SJ, Kim EM, Yamamoto M, et al. Engineering Multi-Cellular Spheroids for Tissue Engineering and Regenerative Medicine. *Adv Healthc Mater* 2020: e2000608. 2020/08/01. DOI: 10.1002/adhm.202000608.
21. Heo DN, Hospodiuk M and Ozbolat IT. Synergistic interplay between human MSCs and HUVECs in 3D spheroids laden in collagen/fibrin hydrogels for bone tissue engineering. *Acta Biomater* 2019; 95: 348-356. 2019/03/05. DOI: 10.1016/j.actbio.2019.02.046.
22. Yang Y, Bajaj N, Xu P, et al. Development of highly porous large PLGA microparticles for pulmonary drug delivery. *Biomaterials* 2009; 30: 1947-1953. 2009/01/13. DOI: 10.1016/j.biomaterials.2008.12.044.

23. Galiakberova AA and Dashinimaev EB. Neural Stem Cells and Methods for Their Generation From Induced Pluripotent Stem Cells in vitro. *Front Cell Dev Biol* 2020; 8: 815. 2020/10/30. DOI: 10.3389/fcell.2020.00815.
24. Gjorevski N, Ranga A and Lutolf MP. Bioengineering approaches to guide stem cell-based organogenesis. *Development* 2014; 141: 1794-1804. 2014/04/24. DOI: 10.1242/dev.101048.
25. Huch M, Knoblich JA, Lutolf MP, et al. The hope and the hype of organoid research. *Development* 2017; 144: 938-941. 2017/03/16. DOI: 10.1242/dev.150201.
26. Jensen G, Morrill C and Huang Y. 3D tissue engineering, an emerging technique for pharmaceutical research. *Acta Pharm Sin B* 2018; 8: 756-766. 2018/09/28. DOI: 10.1016/j.apsb.2018.03.006.
27. Lancaster MA and Knoblich JA. Organogenesis in a dish: modeling development and disease using organoid technologies. *Science* 2014; 345: 1247125. DOI: 10.1126/science.1247125.
28. Yu X, Dillon GP and Bellamkonda RB. A laminin and nerve growth factor-laden three-dimensional scaffold for enhanced neurite extension. *Tissue Eng* 1999; 5: 291-304. 1999/09/09. DOI: 10.1089/ten.1999.5.291.
29. Horch RE, Weigand A, Wajant H, et al. [Biofabrication: new approaches for tissue regeneration]. *Handchir Mikrochir Plast Chir* 2018; 50: 93-100. 2018/01/30. DOI: 10.1055/s-0043-124674.
30. Ariga K. Progress in Molecular Nanoarchitectonics and Materials Nanoarchitectonics. *Molecules* 2021; 26 2021/04/04. DOI: 10.3390/molecules26061621.
31. Ariga K. Nanoarchitectonics: what's coming next after nanotechnology? *Nanoscale Horiz* 2021; 6: 364-378. 2021/05/06. DOI: 10.1039/d0nh00680g.
32. Qutachi O, Vetsch JR, Gill D, et al. Injectable and porous PLGA microspheres that form highly porous scaffolds at body temperature. *Acta Biomater* 2014; 10: 5090-5098. 2014/08/26. DOI: 10.1016/j.actbio.2014.08.015.
33. Kokubo T and Takadama H. How useful is SBF in predicting in vivo bone bioactivity? *Biomaterials* 2006; 27: 2907-2915. 2006/02/02. DOI: 10.1016/j.biomaterials.2006.01.017.
34. Yao Q, Sandhurst ES, Liu Y, et al. BBP-Functionalized Biomimetic Nanofibrous Scaffold Can Capture BMP2 and Promote Osteogenic Differentiation. *J Mater Chem B* 2017; 5: 5196-5205. 2017/12/19. DOI: 10.1039/C7TB00744B.
35. Cheng MT, Yang HW, Chen TH, et al. Modulation of proliferation and differentiation of human anterior cruciate ligament-derived stem cells by different growth factors. *Tissue Eng Part A* 2009; 15: 3979-3989. 2009/07/10. DOI: 10.1089/ten.TEA.2009.0172.
36. Grazul-Bilska AT, Johnson ML, Bilski JJ, et al. Wound healing: the role of growth factors. *Drugs Today (Barc)* 2003; 39: 787-800. 2003/12/12. DOI: 10.1358/dot.2003.39.10.799472.
37. W.C. Oliver GMP. Measurement of hardness and elastic modulus by instrumented indentation: Advances in understanding and refinements to methodology. *Journal of Materials Research* 2004; 19: 3-20. Review.
38. W.C. Oliver GMP. An Improved Technique for Determining Hardness and Elastic Modulus Using Load Displacement Sensing Indentation Experiments. *Journal of Materials Research* 1992; 7: 1564-1583. DOI: https://doi.org/10.1557/JMR.1992.1564.
39. Kar S, Katti DR and Katti KS. Evaluation of quasi-static and dynamic nanomechanical properties of bone-metastatic breast cancer cells using a nanoclay cancer testbed. *Sci Rep* 2021; 11: 3096. 2021/02/06. DOI: 10.1038/s41598-021-82664-9.
40. Molla MS, Katti DR and Katti KS. Mechanobiological evaluation of prostate cancer metastasis to bone using an in vitro prostate cancer testbed. *J Biomech* 2021; 114: 110142. 2020/12/09. DOI: 10.1016/j.jbiomech.2020.110142.

41. Francis KR, Ton AN, Xin Y, et al. Modeling Smith-Lemli-Opitz syndrome with induced pluripotent stem cells reveals a causal role for Wnt/beta-catenin defects in neuronal cholesterol synthesis phenotypes. *Nat Med* 2016; 22: 388-396. 2016/03/22. DOI: 10.1038/nm.4067.
42. Malik N, Wang X, Shah S, et al. Comparison of the gene expression profiles of human fetal cortical astrocytes with pluripotent stem cell derived neural stem cells identifies human astrocyte markers and signaling pathways and transcription factors active in human astrocytes. *PLoS One* 2014; 9: e96139. DOI: 10.1371/journal.pone.0096139.
43. Hung CH and Young TH. Differences in the effect on neural stem cells of fetal bovine serum in substrate-coated and soluble form. *Biomaterials* 2006; 27: 5901-5908. 2006/09/02. DOI: 10.1016/j.biomaterials.2006.08.009.
44. Sawyer AA, Hennessy KM and Bellis SL. Regulation of mesenchymal stem cell attachment and spreading on hydroxyapatite by RGD peptides and adsorbed serum proteins. *Biomaterials* 2005; 26: 1467-1475. 2004/11/04. DOI: 10.1016/j.biomaterials.2004.05.008.
45. Fang CY, Wu CC, Fang CL, et al. Long-term growth comparison studies of FBS and FBS alternatives in six head and neck cell lines. *PLoS One* 2017; 12: e0178960. 2017/06/08. DOI: 10.1371/journal.pone.0178960.
46. Hemeda H, Giebel B and Wagner W. Evaluation of human platelet lysate versus fetal bovine serum for culture of mesenchymal stromal cells. *Cytotherapy* 2014; 16: 170-180. 2014/01/21. DOI: 10.1016/j.jcyt.2013.11.004.
47. Hu BY and Zhang SC. Directed differentiation of neural-stem cells and subtype-specific neurons from hESCs. *Methods Mol Biol* 2010; 636: 123-137. 2010/03/26. DOI: 10.1007/978-1-60761-691-7_8.
48. Schulz TC, Noggle SA, Palmarini GM, et al. Differentiation of human embryonic stem cells to dopaminergic neurons in serum-free suspension culture. *Stem Cells* 2004; 22: 1218-1238. 2004/12/08. DOI: 10.1634/stemcells.2004-0114.
49. Chuang JH, Tung LC and Lin Y. Neural differentiation from embryonic stem cells in vitro: An overview of the signaling pathways. *World J Stem Cells* 2015; 7: 437-447. 2015/03/31. DOI: 10.4252/wjsc.v7.i2.437.
50. Fang Y and Eglen RM. Three-Dimensional Cell Cultures in Drug Discovery and Development. *SLAS DISCOVERY: Advancing Life Sciences R&D* 2017. DOI: 10.1177/2472555217696795.
51. Hughes CS, Postovit LM and Lajoie GA. Matrigel: a complex protein mixture required for optimal growth of cell culture. *Proteomics* 2010; 10: 1886-1890. 2010/02/18. DOI: 10.1002/pmic.200900758.
52. Scholzen T and Gerdes J. The Ki-67 protein: from the known and the unknown. *J Cell Physiol* 2000; 182: 311-322. 2000/02/01. DOI: 10.1002/(SICI)1097-4652(200003)182:3<311::AID-JCP1>3.0.CO;2-9.
53. Melissaridou S, Wiechec E, Magan M, et al. The effect of 2D and 3D cell cultures on treatment response, EMT profile and stem cell features in head and neck cancer. *Cancer Cell Int* 2019; 19: 16. 2019/01/18. DOI: 10.1186/s12935-019-0733-1.
54. Li X, Chu J, Wang A, et al. Uniaxial mechanical strain modulates the differentiation of neural crest stem cells into smooth muscle lineage on micropatterned surfaces. *PLoS One* 2011; 6: e26029. 2011/10/22. DOI: 10.1371/journal.pone.0026029.
55. Porter FD and Herman GE. Malformation syndromes caused by disorders of cholesterol synthesis. *J Lipid Res* 2011; 52: 6-34. Research Support, N.I.H., Extramural

Research Support, N.I.H., Intramural

Review 2010/10/12. DOI: 10.1194/jlr.R009548.
56. Pham MT, Pollock KM, Rose MD, et al. Generation of human vascularized brain organoids. *Neuroreport* 2018; 29: 588-593. 2018/03/24. DOI: 10.1097/WNR.0000000000001014.

57. Shafiee S, Shariatzadeh S, Zafari A, et al. Recent Advances on Cell-Based Co-Culture Strategies for Prevascularization in Tissue Engineering. *Front Bioeng Biotechnol* 2021; 9: 745314. 2021/12/14. DOI: 10.3389/fbioe.2021.745314.
58. Risau W and Flamme I. Vasculogenesis. *Annu Rev Cell Dev Biol* 1995; 11: 73-91. 1995/01/01. DOI: 10.1146/annurev.cb.11.110195.000445.
59. Santos C, Gomes P, Duarte JA, et al. Development of hydroxyapatite nanoparticles loaded with folic acid to induce osteoblastic differentiation. *Int J Pharm* 2017; 516: 185-195. 2016/11/17. DOI: 10.1016/j.ijpharm.2016.11.035.
60. Bodhak S, de Castro LF, Kuznetsov SA, et al. Combinatorial cassettes to systematically evaluate tissue-engineered constructs in recipient mice. *Biomaterials* 2018; 186: 31-43. 2018/10/03. DOI: 10.1016/j.biomaterials.2018.09.035.
61. Kuznetsov SA, Cherman N and Robey PG. In vivo bone formation by progeny of human embryonic stem cells. *Stem Cells Dev* 2011; 20: 269-287. 2010/07/02. DOI: 10.1089/scd.2009.0501.
62. Hao M, Zhang Z, Liu C, et al. Hydroxyapatite Nanorods Function as Safe and Effective Growth Factors Regulating Neural Differentiation and Neuron Development. *Adv Mater* 2021; 33: e2100895. 2021/07/12. DOI: 10.1002/adma.202100895.
63. Shen Y, Liu F, Duan J, et al. Biomaterial Cues Regulated Differentiation of Neural Stem Cells into GABAergic Neurons through Ca(2+)/c-Jun/TLX3 Signaling Promoted by Hydroxyapatite Nanorods. *Nano Lett* 2021; 21: 7371-7378. 2021/08/24. DOI: 10.1021/acs.nanolett.1c02708.
64. Loh QL and Choong C. Three-dimensional scaffolds for tissue engineering applications: role of porosity and pore size. *Tissue Eng Part B Rev* 2013; 19: 485-502. 2013/05/16. DOI: 10.1089/ten.TEB.2012.0437.
65. Makadia HK and Siegel SJ. Poly Lactic-co-Glycolic Acid (PLGA) as Biodegradable Controlled Drug Delivery Carrier. *Polymers (Basel)* 2011; 3: 1377-1397. 2012/05/12. DOI: 10.3390/polym3031377.
66. Krishna L, Dhamodaran K, Jayadev C, et al. Nanostructured scaffold as a determinant of stem cell fate. *Stem Cell Res Ther* 2016; 7: 188. 2017/01/01. DOI: 10.1186/s13287-016-0440-y.
67. Kim SH, Kim JE, Kim SH, et al. Substance P/dexamethasone-encapsulated PLGA scaffold fabricated using supercritical fluid process for calvarial bone regeneration. *J Tissue Eng Regen Med* 2017; 11: 3469-3480. 2017/06/02. DOI: 10.1002/term.2260.
68. Raeisdasteh Hokmabad V, Davaran S, Ramazani A, et al. Design and fabrication of porous biodegradable scaffolds: a strategy for tissue engineering. *J Biomater Sci Polym Ed* 2017; 28: 1797-1825. 2017/07/15. DOI: 10.1080/09205063.2017.1354674.
69. Davies JE, Matta R, Mendes VC, et al. Development, characterization and clinical use of a biodegradable composite scaffold for bone engineering in oro-maxillo-facial surgery. *Organogenesis* 2010; 6: 161-166. 2011/01/05. DOI: 10.4161/org.6.3.12392.
70. Papadimitriou L, Manganas P, Ranella A, et al. Biofabrication for neural tissue engineering applications. *Mater Today Bio* 2020; 6: 100043. 2020/03/20. DOI: 10.1016/j.mtbio.2020.100043.
71. Yamagata K, Nakayamada S and Tanaka Y. Use of mesenchymal stem cells seeded on the scaffold in articular cartilage repair. *Inflamm Regen* 2018; 38: 4. 2018/03/22. DOI: 10.1186/s41232-018-0061-1.
72. Zhuang P, Sun AX, An J, et al. 3D neural tissue models: From spheroids to bioprinting. *Biomaterials* 2018; 154: 113-133. 2017/11/10. DOI: 10.1016/j.biomaterials.2017.10.002.
73. Clark A, Milbrandt TA, Hilt JZ, et al. Tailoring properties of microsphere-based poly(lactic-co-glycolic acid) scaffolds. *J Biomed Mater Res A* 2014; 102: 348-357. 2013/03/28. DOI: 10.1002/jbm.a.34706.
74. Keles H, Naylor A, Clegg F, et al. Investigation of factors influencing the hydrolytic degradation of single PLGA microparticles. *Polymer Degradation and Stability* 2015; 119: 228-241. DOI: 10.1016/j.polymdegradstab.2015.04.025.

75. Kranz H, Ubrich N, Maincent P, et al. Physicomechanical properties of biodegradable poly(D,L-lactide) and poly(D,L-lactide-co-glycolide) films in the dry and wet states. *J Pharm Sci* 2000; 89: 1558-1566. 2000/10/24. DOI: 10.1002/1520-6017(200012)89:12<1558::aid-jps6>3.0.co;2-8.
76. Hazeltine LB, Selekman JA and Palecek SP. Engineering the human pluripotent stem cell microenvironment to direct cell fate. *Biotechnol Adv* 2013; 31: 1002-1019. 2013/03/21. DOI: 10.1016/j.biotechadv.2013.03.002.
77. Yakoub AM and Sadek M. Development and Characterization of Human Cerebral Organoids: An Optimized Protocol. *Cell Transplant* 2018; 27: 393-406. 2018/05/12. DOI: 10.1177/0963689717752946.
78. Langhans SA. Three-Dimensional in Vitro Cell Culture Models in Drug Discovery and Drug Repositioning. *Front Pharmacol* 2018; 9: 6. 2018/02/08. DOI: 10.3389/fphar.2018.00006.
79. Marti-Figueroa CR and Ashton RS. The case for applying tissue engineering methodologies to instruct human organoid morphogenesis. *Acta Biomater* 2017; 54: 35-44. 2017/03/21. DOI: 10.1016/j.actbio.2017.03.023.
80. Vieira MS, Santos AK, Vasconcellos R, et al. Neural stem cell differentiation into mature neurons: Mechanisms of regulation and biotechnological applications. *Biotechnol Adv* 2018; 36: 1946-1970. 2018/08/06. DOI: 10.1016/j.biotechadv.2018.08.002.
81. Verma I, Rashid Z, Sikdar SK, et al. Efficient neural differentiation of mouse pluripotent stem cells in a serum-free medium and development of a novel strategy for enrichment of neural cells. *Int J Dev Neurosci* 2017; 61: 112-124. 2017/07/05. DOI: 10.1016/j.ijdevneu.2017.06.009.
82. Hellwig C, Barenys M, Baumann J, et al. Culture of human neurospheres in 3D scaffolds for developmental neurotoxicity testing. *Toxicol In Vitro* 2018; 52: 106-115. 2018/06/09. DOI: 10.1016/j.tiv.2018.06.002.
83. Koh HS, Yong T, Chan CK, et al. Enhancement of neurite outgrowth using nano-structured scaffolds coupled with laminin. *Biomaterials* 2008; 29: 3574-3582. 2008/06/06. DOI: 10.1016/j.biomaterials.2008.05.014.
84. Chou MJ, Hsieh CH, Yeh PL, et al. Application of open porous poly(D,L-lactide-co-glycolide) microspheres and the strategy of hydrophobic seeding in hepatic tissue cultivation. *J Biomed Mater Res A* 2013; 101: 2862-2869. 2013/03/19. DOI: 10.1002/jbm.a.34594.
85. Kang SW and Bae YH. Cryopreservable and tumorigenic three-dimensional tumor culture in porous poly(lactic-co-glycolic acid) microsphere. *Biomaterials* 2009; 30: 4227-4232. 2009/05/19. DOI: 10.1016/j.biomaterials.2009.04.025.
86. Jakobsson A, Ottosson M, Zalis MC, et al. Three-dimensional functional human neuronal networks in uncompressed low-density electrospun fiber scaffolds. *Nanomedicine* 2017; 13: 1563-1573. 2017/01/09. DOI: 10.1016/j.nano.2016.12.023.
87. Sensharma P, Madhumathi G, Jayant RD, et al. Biomaterials and cells for neural tissue engineering: Current choices. *Mater Sci Eng C Mater Biol Appl* 2017; 77: 1302-1315. 2017/05/24. DOI: 10.1016/j.msec.2017.03.264.
88. Hofrichter M, Nimtz L, Tigges J, et al. Comparative performance analysis of human iPSC-derived and primary neural progenitor cells (NPC) grown as neurospheres in vitro. *Stem Cell Res* 2017; 25: 72-82. 2017/11/08. DOI: 10.1016/j.scr.2017.10.013.
89. Martens YA, Xu S, Tait R, et al. Generation and validation of APOE knockout human iPSC-derived cerebral organoids. *STAR Protoc* 2021; 2: 100571. 2021/06/22. DOI: 10.1016/j.xpro.2021.100571.
90. Pasca SP. Assembling human brain organoids. *Science* 2019; 363: 126-127. 2019/01/12. DOI: 10.1126/science.aau5729.
91. Marton RM and Pasca SP. Organoid and Assembloid Technologies for Investigating Cellular Crosstalk in Human Brain Development and Disease. *Trends Cell Biol* 2019 2019/12/28. DOI: 10.1016/j.tcb.2019.11.004.

92. Wang X, Wenk E, Zhang X, et al. Growth factor gradients via microsphere delivery in biopolymer scaffolds for osteochondral tissue engineering. *J Control Release* 2009; 134: 81-90. 2008/12/17. DOI: 10.1016/j.jconrel.2008.10.021.